



Non-Markovian decoherence dynamics of strong-coupling hybrid quantum systems: A master equation approach

Kai-Ting Chiang  and Wei-Min Zhang **Department of Physics and Center for Quantum Information Science, National Cheng Kung University, Tainan 70101, Taiwan*

(Received 6 July 2020; accepted 22 December 2020; published 11 January 2021)

Based on the experiments [S. Putz *et al.*, *Nat. Phys.* **10**, 720 (2014); *Nat. Photonics* **11**, 36 (2017)] on the hybrid quantum system of a superconducting microwave cavity coupled strongly to an inhomogeneous broadening spin ensemble, we use the exact master equation theory to investigate its non-Markovian decoherence dynamics under external driving fields. In the experiments, the spin ensemble is made of negatively charged nitrogen-vacancy defects in diamond. The exact master equation theory generalizes the fluctuation-dissipation relation and depicts in details the transient non-Markovian decoherence, in which the dissipation (relaxation) and fluctuations (noise or dephasing) dynamics is well described and the non-Markovian memory effect can be well characterized. We study the physical picture of the transient non-Markovian decoherence dynamics and explore how the non-Markovian decoherence induced by the inhomogeneous broadening of the spin ensemble is suppressed in the strong-coupling regime. We also show how the spectral hole burning generates localized bound states for the further decoherence suppression. Furthermore, we investigate the two-time correlations to show the relationships between quantum fluctuations and quantum memory.

DOI: [10.1103/PhysRevA.103.013714](https://doi.org/10.1103/PhysRevA.103.013714)

I. INTRODUCTION

Cavity quantum electrodynamics (QED) is a main research topic for individual quantum system controlling and for quantum information storage and transmission in quantum information technology [1]. It has also attracted great attention in the study of the fundamental quantum theory of open systems and the measurement-induced decoherence dynamics [2]. Cavity QED studies properties of atoms coupled to discrete photon modes in cavities. Since the early 1980s, the investigation of cavity QED has moved towards strong-coupling regime with high-quality factor cavities [1,3]. The strong-coupling cavity QED has been experimentally realized in a multitude of physical systems, including Rydberg atoms in microwave cavities [4,5], alkali-metal atoms in optical cavities [6–8], and superconducting circuits [9,10], etc. In some circumstance, decoherence (coherence loss) of photon and atom states can be effectively suppressed in strong-coupling cavity QED, and single-photon and single-atom states can be dynamically manipulated.

A particular important realization of strong-coupling cavity QED is the hybrid quantum systems of large spin or atom ensembles coupled to microwave cavities [4,5,11], where the collective coupling strength is proportional to the square root of the number of emitters. The spin or atomic ensemble may also play the role of quantum memories that quantum information can be coherently stored and retrieved at some later time. Such hybrid systems have been realized in various spin ensembles, such as negatively charged nitrogen-vacancy (NV) defects in diamond [12,13], rare-earth spin ensembles [14],

and magnons in yttrium iron garnet [15,16], etc. In particular, the NV centers in diamond have the long coherence time even at room temperature, and therefore show the great potential for their applications in quantum information processing and storage. The strong coupling of such spin ensembles with microwave cavities could make coherent transfer of quantum information between cavities and spin ensembles more feasible.

However, due to the local magnetic dipole-dipole couplings between NV centers and the residual nitrogen paramagnetic impurities, the resonance line of a large NV electron spin ensemble is inhomogeneously broadened [17–20]. Inhomogeneous spin ensemble broadening could induce decoherence to the cavity photons, which may limit the performance of the coherent transfer and storage of quantum information. It was found that in the strong-coupling regime, inhomogeneous broadening induced decoherence may be suppressed upon the width and shape of the inhomogeneous broadening, which is called as “cavity protection effect” in the literature [18,19]. At the same time or even earlier, we have found another mechanism of decoherence suppression in nano-cavities strongly coupled to photonic crystals, due to the existence of localized bound states associated with tight-binding spectral density [21–23]. Such decoherence suppression mechanism was solved from the exact master equation theory we developed [24–28]. Recently, Putz *et al.* have experimentally demonstrated both phenomena of decoherence suppressions in the real-time dynamics of a superconducting microwave cavity coupled strongly to the spin ensemble of NV centers [29,30]. By appropriately choosing microwave pulses, they can increase the amplitude of coherent oscillations between the cavity and the spin ensemble. They also used the semiclassical approach in terms of Volterra equation which

*wzhang@mail.ncku.edu.tw

is a governing equation for cavity field decays [31–34] to explain their experimental observation. In this paper, we will study the transient dynamics of such hybrid quantum systems using our exact master equation theory [24–28]. With the master equation formulation, dissipation (relaxation) and fluctuations (noise or dephasing) dynamics can be consistently characterized, and non-Markovian memory can be physically quantified. New insights on the transient non-Markovian decoherence dynamics and decoherence suppressions in strong-coupling hybrid quantum systems can also be obtained in a more general and complete manner.

The experimental system [29,30] of the superconducting microwave cavity coupled strongly to the spin ensemble of NV centers can be described by the Tavis-Cummings model [35]. In this paper, we will use the Tavis-Cummings model to investigate the decoherence dynamics of cavity QED arising from the spin ensemble. Such decoherence dynamics heavily involves non-Markovian memory processes. The Tavis-Cummings model of the spin ensemble at arbitrary temperature cannot be solved exactly. However, the experimental setup for a high-polarization spin ensemble, i.e., only a small percentage of spins ($\approx 10^6$) are excited in comparison with the total spin number ($\approx 10^{12}$) in the ensemble, enables one to effectively convert the spin ensemble into a bosonic ensemble under the Holstein-Primakoff approximation [18,19,36]. With such a treatment, we can derive the exact master equation. Then, we can systematically study the non-Markovian dynamics of this hybrid system under external driving fields [26,27]. We can also address rigorously quantum dissipation and thermal fluctuation together to depict the transient non-Markovian decoherence dynamics. It provides an interesting physical picture of how the decoherence induced by inhomogeneous broadening is suppressed in the strong-coupling regime. Moreover, we show that the spectral hole burning generates localized bound states (localized modes) between the cavity and the spin ensemble, which further suppresses the decoherence [21–23]. We also use two time-correlation functions to explore quantum memory effect [37–39].

The rest of the paper is organized as follows. In Sec. II, we discuss the general master equation theory to hybrid quantum systems. We begin with the generalized Tavis-Cummings model for the hybrid quantum system of a superconducting microwave cavity coupled strongly to a spin ensemble of NV centers. Under the experimental setup and applying the Holstein-Primakoff approximation to the spin ensemble, we have the exact master equation for the cavity system under external driving fields we derived early [26]. We also discuss in details the physical consequence of the dissipation and fluctuations from the master equation, from which the physical picture of non-Markovian memory processes is provided for open quantum systems. We further explore how the noise correlation functions characterize quantum memory. In Secs. III and Sec. IV, we apply the theory to study the decoherence dynamics of the cavity field and make comparison with the experiment observations and other theoretical methods for different setups of the spin ensemble in experiments [29,30], where the origin of non-Markovian decoherence dynamics and the different mechanisms of decoherence suppression are analyzed in details. In Sec. V, we use the time-correlation functions to study the new feature of quantum memory for

the further experimental measurement. A conclusion of this work and the perspective for the further researches are given in Sec. VI.

II. HYBRID QUANTUM SYSTEM AND THE EXACT MASTER EQUATION METHOD

A. Tavis-Cummings model with external driving field

The hybrid quantum system studied in experiments [29,30] consists of a superconducting microwave cavity coupled to a spin ensemble of NV centers. The cavity is also driven by a microwave pulse. This system can be described by a generalized Tavis-Cummings model with the following Hamiltonian:

$$H(t) = \hbar\omega_c a^\dagger a + [f(t)a^\dagger + f^*(t)a] + \sum_k [\Delta_k \sigma_k^z + V_k a^\dagger \sigma_k^- + V_k^* \sigma_k^+ a] + \sum_l [\hbar\omega_l b_l^\dagger b_l + V_l a^\dagger b_l + V_l^* b_l^\dagger a]. \quad (1)$$

Here, the first term describes a single-mode cavity, and a^\dagger (a) is the corresponding bosonic creation (annihilation) operator with ω_c being the resonant frequency. The second term describes the microwave pulse driving field applying on the cavity $f(t) = \eta(t)e^{-i\omega_p t}$, where $\eta(t)$ is the time-dependent field strength and ω_p is the phase frequency. The driving pulse is used to control the dynamics of the hybrid system through the cavity. The third term is the Hamiltonian of the spin ensemble of NV centers and its coupling with the cavity, where σ_k^z , σ_k^\pm are the three Pauli matrices, Δ_k is the corresponding two-level energy splitting, and V_k is the coupling amplitude between the cavity and the spin mode k . The remaining Hamiltonian describes the cavity leakage, where b_l^\dagger (b_l) is the creation (annihilation) operator of the photonic mode l in the electromagnetic (EM) environment in free space with frequency ω_l , and V_l is the coupling amplitude between the cavity and the EM environmental mode l .

In the experimental setup [29,30], only a small percentage of spins ($\approx 10^6$) are excited in comparison with the total spin number ($\approx 10^{12}$) in the ensemble. This corresponds to a high-polarization spin ensemble [18]. Thus, the Holstein-Primakoff approximation [36]

$$\sigma_k^z \equiv c_k^\dagger c_k - 1/2, \quad \sigma_k^+ \equiv c_k^\dagger \sqrt{1 - c_k^\dagger c_k} \simeq c_k^\dagger \quad (2)$$

can be applied to the spin variables, where c_k^\dagger , c_k are the bosonic creation and annihilation operators of the corresponding spin mode k . As a result, the Hamiltonian (3) can be reduced to

$$H = \hbar\omega_c a^\dagger a + [f(t)a^\dagger + f^*(t)a] + \sum_k [\Delta_k c_k^\dagger c_k + V_k a^\dagger c_k + V_k^* c_k^\dagger a] + \sum_l [\hbar\omega_l b_l^\dagger b_l + V_l a^\dagger b_l + V_l^* b_l^\dagger a], \quad (3)$$

which can provide a good accuracy to the experimental observations, as one will see later. Now, the dynamics of the hybrid quantum system (the cavity, the spin ensemble, and the EM

environment) can be exactly solved. Usually, decoherence of photon states due to photon leakages and atomic absorptions can be treated with constant decay rates (Markov decoherence phenomena) [2]. However, for the strong-coupling cavity QED system with the spin ensemble, the resonance line of the NV spin ensemble is inhomogeneously broadened so that non-Markovian decoherence dominates the photon dynamics in this hybrid quantum system. Therefore, a more casual treatment to open quantum system dynamics is demanded.

B. Non-Markovian decoherence theory based on exact master equation

In principle, the dynamics of the total systems (the cavity system, the spin ensemble, and the EM environmental modes) is given by the total density matrix under the unitary evolution

$$\rho_{\text{tot}}(t) = U(t, t_0)\rho_{\text{tot}}(t_0)U^\dagger(t, t_0), \quad (4)$$

where $U(t, t_0) = \mathcal{T} \exp(\frac{1}{i\hbar} \int_{t_0}^t d\tau H(\tau))$ is the unitary evolution operator of the total system, and \mathcal{T} is the time-ordering operator. Initially, the density matrix of the cavity state $\rho_c(t_0)$ can be arbitrary, the spin ensemble and the EM environment are in the partitioned thermal state $\rho_{\text{tot}}(t_0) = \rho_c(t_0) \otimes \rho_s(t_0) \otimes \rho_e(t_0)$, where $\rho_s(t_0) = \frac{1}{Z_s} e^{-\beta_s \sum_k \Delta_k \sigma_k^z}$ and $\rho_e(t_0) = \frac{1}{Z_e} e^{-\beta_e \sum_l \hbar \omega_l b_l^\dagger b_l}$, where $\beta_s = 1/(kT_s)$ and $\beta_e = 1/(kT_e)$ are the inverse of their initial temperatures which could be the same or different. Immediately after the time t_0 , the cavity, the spin ensemble, and the environment evolve into a nonequilibrium state under Eq. (4). Experimentally, one only measures the physical observables of the cavity system, such as the cavity field intensity (photon numbers) and photon correlations. Therefore, we shall focus on the cavity photon state dynamics only, which is determined by the reduced density matrix which is defined by

$$\rho_c(t) = \text{Tr}_{s+e}[\rho_{\text{tot}}(t)], \quad (5)$$

and the notation Tr_{s+e} is the trace over all the states of the spin ensemble and the EM environment. The reduced density matrix encompasses all the influences arisen from the spin ensemble and the EM environment after we take the trace over the spin and EM environmental states.

To study the non-Markovian decoherence dynamics of the system, we apply the exact master equation theory developed recently [24–28], which has been used in many applications to various different systems [21–23, 38, 40–44]. After we traced out all the spin and environmental states from Eq. (4) using the coherent state path integral [45], we obtain the exact master equation for the reduced density matrix of the cavity system [26]:

$$\begin{aligned} \frac{d}{dt} \rho_c(t) = & \frac{1}{i\hbar} [\omega'_c(t, t_0) a^\dagger a + f'^*(t, t_0) a + f'(t, t_0) a^\dagger, \rho_c(t)] \\ & + \gamma(t, t_0) [2a\rho_c(t)a^\dagger - a^\dagger a\rho_c(t) - \rho_c(t)a^\dagger a] \\ & + \tilde{\gamma}(t, t_0) [a\rho_c(t)a^\dagger + a^\dagger \rho_c(t)a \\ & - a^\dagger a\rho_c(t) - \rho_c(t)aa^\dagger]. \end{aligned} \quad (6)$$

Here, the first term describes a unitary evolution of cavity photon states. The renormalized cavity frequency $\omega'_c(t, t_0)$ and the renormalized external driving field $f'(t, t_0)$ have taken

into account the influences of the spin ensemble and the EM environment to the cavity state dynamics. The other two terms in the master equation represent the nonunitary evolution due to the dissipation and fluctuations induced also by the spin ensemble and the EM environment. The dissipation and fluctuation dynamics are characterized explicitly with the dissipation and fluctuation coefficients $\gamma(t, t_0)$ and $\tilde{\gamma}(t, t_0)$, respectively. They describe the decay (relaxation) of the cavity field and the dephasing (thermalization) between the cavity and the spin ensemble. The most important feature in the above exact master equation is that the time non-local renormalized cavity frequency $\omega'_c(t, t_0)$, renormalized external driving field $f'(t, t_0)$, dissipation coefficient $\gamma(t, t_0)$, and fluctuation coefficient $\tilde{\gamma}(t, t_0)$ are all determined by the nonequilibrium Green functions [26]

$$i\omega'_c(t, t_0) + \gamma(t, t_0) = -\frac{\dot{u}(t, t_0)}{u(t, t_0)}, \quad (7a)$$

$$f'(t, t_0) = i\dot{y}(t, t_0) - i \left[\frac{\dot{u}(t, t_0)}{u(t, t_0)} y(t, t_0) \right], \quad (7b)$$

$$\tilde{\gamma}(t, t_0) = \lim_{\tau \rightarrow t} \frac{\partial v(\tau, t)}{\partial \tau} - \left[\frac{\dot{u}(t, t_0)}{u(t, t_0)} v(t, t) + \text{c.c.} \right]. \quad (7c)$$

The nonequilibrium Green functions $u(t, t_0)$, $y(t, t_0)$, and $v(\tau, t)$ obey the following integrodifferential equations

$$\frac{d}{dt} u(t, t_0) + i\omega_c u(t, t_0) + \int_{t_0}^t d\tau g(t, \tau) u(\tau, t_0) = 0, \quad (8a)$$

$$\frac{d}{dt} y(t, t_0) + i\omega_c y(t, t_0) + \int_{t_0}^t d\tau g(t, \tau) y(\tau, t_0) = \frac{1}{i\hbar} f(t), \quad (8b)$$

$$\begin{aligned} \frac{d}{d\tau} v(\tau, t) + i\omega_c v(\tau, t) + \int_{t_0}^{\tau} d\tau' g(\tau, \tau') v(\tau', t) \\ = \int_{t_0}^t dt' \tilde{g}(\tau, t') \bar{u}(t', t) \quad (\tau \leq t) \end{aligned} \quad (8c)$$

subjected to the boundary conditions $u(t_0, t_0) = 1$, $y(t_0, t_0) = 0$, and $v(t_0, t) = 0$. In Eq. (8), the memory integral kernels $g(t, \tau)$ and $\tilde{g}(t, \tau)$ are defined by

$$\begin{aligned} g(t, \tau) = & \frac{1}{\hbar^2} \sum_k |V_k|^2 e^{-i\Delta_k(t-\tau)/\hbar} + \frac{1}{\hbar^2} \sum_l |V_l|^2 e^{-i\omega_l(t-\tau)} \\ = & \sum_{\alpha=s,e} \int_0^\infty \frac{d\omega}{2\pi} J_\alpha(\omega) e^{-i\omega(t-\tau)}, \end{aligned} \quad (9a)$$

$$\begin{aligned} \tilde{g}(t, \tau) = & \frac{1}{\hbar^2} \sum_k |V_k|^2 \bar{n}(\Delta_k/\hbar, T_s) e^{-i\Delta_k(t-\tau)/\hbar} \\ & + \frac{1}{\hbar^2} \sum_l |V_l|^2 \bar{n}(\omega_l, T_e) e^{-i\omega_l(t-\tau)} \\ = & \sum_{\alpha=s,e} \int_0^\infty \frac{d\omega}{2\pi} J_\alpha(\omega) \bar{n}(\omega, T_\alpha) e^{-i\omega(t-\tau)}, \end{aligned} \quad (9b)$$

where

$$J_s(\omega) = \frac{2\pi}{\hbar^2} \sum_k |V_k|^2 \delta(\omega - \Delta_k/\hbar), \quad (10a)$$

$$J_e(\omega) = \frac{2\pi}{\hbar^2} \sum_l |V_l|^2 \delta(\omega - \omega_l) \simeq 2\kappa \quad (10b)$$

are the spectral densities associated with the spin ensemble and the EM environment, respectively, and $\bar{n}(\omega, T_{s,e}) = 1/(e^{\hbar\omega/kT_{s,e}} - 1)$ are the corresponding particle distribution function. The frequency dependence of $J_s(\omega)$ depicts the inhomogeneous broadening of the spin ensemble spectrum. The cavity decay rate κ characterizes the cavity leakage effect.

The above formulation shows that after trace over all the spin ensemble and the EM environmental states, the influence of the spin ensemble to the cavity state dynamics is fully encapsulated in the spectral density $J_s(\omega)$. In particular, the dissipation and fluctuation coefficients $\gamma(t, t_0)$ and $\tilde{\gamma}(t, t_0)$ provide a complete description of decay (relaxation) and dephasing (thermalization) of the decoherence dynamics under the given spectral density $J_s(\omega)$. We can further simplify the integrodifferential equation of $u(t, t_0)$ as

$$\begin{aligned} \frac{d}{dt} u(t, t_0) + (i\omega_c + \kappa)u(t, t_0) \\ = - \int_{t_0}^t d\tau \int_0^\infty \frac{d\omega}{2\pi} J_s(\omega) e^{-i\omega(t-\tau)} u(\tau, t_0). \end{aligned} \quad (11)$$

As one can see, without the spin ensemble, the solution of the above equation is $u(t, t_0) = e^{-(i\omega_c + \kappa)(t-t_0)}$. It simply describes the spontaneous decay of the cavity field, as one expected. The last term in Eq. (11) determines the dissipation dynamics of the cavity photons arisen from the spin ensemble. Notice that the dissipation coefficient $\gamma(t, t_0)$ is only determined by the $u(t, t_0)$, namely, it only describes the decay dynamics of the system.

Furthermore, because of the boundary conditions $y(t_0, t_0) = 0$ and $v(t_0, t) = 0$, Eqs. (8c) and (8b) can be analytically solved in terms of $u(t, t_0)$ [26]:

$$y(t, t_0) = \frac{1}{i\hbar} \int_{t_0}^t d\tau u(t, \tau) f(\tau), \quad (12a)$$

$$v(\tau, t) = \int_{t_0}^\tau dt_1 \int_{t_0}^{t_1} dt_2 u(\tau, t_1) \tilde{g}(t_1, t_2) u^\dagger(t, t_2). \quad (12b)$$

It shows that $y(t, t_0)$ is the cavity response field with respect to the driving field $f(t)$ incorporating the dissipation effect of the spin ensemble. Furthermore, the Green function $v(\tau, t)$ is the correlation associated with the initial state of the spin ensemble, which is indeed the noise correlation characterizing the dephasing process and the non-Markovian memory dynamics, as we will see later from Eq. (20) and the discussion thereafter.

Now, using the exact master equation, we can easily compute the experimentally measurable cavity field $\langle a(t) \rangle = \text{Tr}[a\rho_c(t)]$ or cavity intensity (cavity photon number) $\langle n(t) \rangle = \text{Tr}[a^\dagger a\rho_c(t)]$:

$$\langle a(t) \rangle = u(t, t_0)\langle a(t_0) \rangle + y(t, t_0), \quad (13a)$$

$$\begin{aligned} \langle n(t) \rangle = |u(t, t_0)|^2 \langle a^\dagger(t_0) a(t_0) \rangle + |y(t, t_0)|^2 + v(t, t) \\ + [u^*(t, t_0)\langle a^\dagger(t_0) \rangle y(t, t_0) + \text{c.c.}]. \end{aligned} \quad (13b)$$

The semiclassical method used by Putz *et al.* [29,30] in the explanation of their experimental observations is based on the Volterra integral equation which can be equivalently written as

$$\begin{aligned} \langle n(t) \rangle_{\text{sc}} = |\langle a(t) \rangle|^2 = |u(t, t_0)\langle a(t_0) \rangle + y(t, t_0)|^2 \\ + [u^*(t, t_0)\langle a^\dagger(t_0) \rangle y(t, t_0) + \text{c.c.}]. \end{aligned} \quad (14)$$

The difference between the full quantum mechanical solution given here and the semiclassical solution in Refs. [29,30] is the quantum fluctuations and thermal noises

$$\begin{aligned} \langle n(t) \rangle - \langle n(t) \rangle_{\text{sc}} \\ = v(t, t) + |u(t, t_0)|^2 (\langle a^\dagger(t_0) a(t_0) \rangle - \langle a^\dagger(t_0) \rangle \langle a(t_0) \rangle). \end{aligned} \quad (15)$$

This difference can be negligible in the semiclassical regime [the average photon number $\langle n(t) \rangle \sim 10^6$, as was measured in experiments [29,30]]. However, in the quantum regime, $\langle n(t) \rangle$ can be the order of one or less, where quantum and thermal fluctuations become significant in the study of non-Markovian processes, as we will discuss in the next subsections.

C. Quantum Langevin equation and noise correlation

For a self-consistency check and also for an alternative physical interpretation to the non-Markovian decoherence dynamics given in the master equation, we make the connection of the above result with the quantum Langevin equation derived directly from Heisenberg equation of motion. Using the Heisenberg equation of motion and eliminating the variables of the spin ensemble as well as the EM environmental modes, we have obtained the following quantum Langevin equation [40,42,46,47] for the cavity field operator $a(t)$:

$$\begin{aligned} \frac{d}{dt} a(t) + (i\omega_c + \kappa)a(t) \\ + \int_{t_0}^t d\tau \int_0^\infty \frac{d\omega}{2\pi} J_s(\omega) e^{-i\omega(t-\tau)} a(\tau) = \frac{1}{i\hbar} [f(t) + \xi(t)], \end{aligned} \quad (16)$$

where $\xi(t)$ is the noise force induced by both the spin ensemble and the EM environment:

$$\xi(t) = \sum_k V_k e^{-i\Delta_k(t-t_0)/\hbar} c_k(t_0) + \sum_l V_l e^{-i\omega_l(t-t_0)} b_l(t_0). \quad (17)$$

If one takes the expectation value to the quantum Langevin equation (16), it reproduces the Volterra equation proposed and used in [29,31,32], as a semiclassical approach where the noise force contribution to cavity state dynamics is ignored because $\langle \xi(t) \rangle = 0$. In other words, the Volterra equation can describe the decay (relaxation) process, but is unable to address the noise (dephasing) dynamics induced by the fluctuations or noise forces from the spin ensemble. The fluctuations become significantly important in the study of the two-time photon correlation functions in the small photon-number regime, as will be discussed in Sec. V.

Due to the linearity of Eq. (16), the general solution of the quantum Langevin equation is

$$a(t) = u(t, t_0)a(t_0) + y(t, t_0) + \zeta(t). \quad (18)$$

It is easy to find that $u(t, t_0)$ and $y(t, t_0)$ are given by Eqs. (11) and (12a), and $\zeta(t)$ is the noise response field to the noise force $\xi(t)$:

$$\zeta(t) = \frac{1}{i\hbar} \int_{t_0}^t d\tau u(t, \tau) \xi(\tau). \quad (19)$$

Furthermore, the correlation function $v(t, t)$ of Eq. (12b) obtained in the master equation method is just the noise correlation:

$$\begin{aligned} v(\tau, t) &= \langle \zeta^\dagger(t) \zeta(\tau) \rangle \\ &= \int_{t_0}^\tau dt_1 \int_{t_0}^t dt_2 u(\tau, t_1) \tilde{g}(t_1, t_2) u^\dagger(t, t_2). \end{aligned} \quad (20)$$

Thus, we reproduce the Green functions $u(t, t_0)$, $v(\tau, t)$ and the driving-field induced cavity response field $y(t, t_0)$ in the exact master equation. In particular, Eq. (20) is the nonequilibrium generalization of the fluctuation-dissipation theorem in the time domain. In other words, in the full quantum mechanical description of open quantum systems, dissipation (relaxation) and fluctuations (noise or dephasing) are simultaneously related to each other, and should be put together in the study of the non-Markovian memory dynamics, as we will discuss next.

D. Noise correlations and the nature of non-Markovian dynamics

Non-Markovian dynamics is a memory feature characterizing the correlations between the system and the environment during their historical evolution. It is the convolution integrals (with the memory kernels) in Eqs. (11) and (20) that depict the non-Markovian dynamics of the cavity system interacting with the spin ensemble. The non-Markovian cavity dissipation dynamics is determined by the Green function $u(t, t_0)$ of Eq. (11). Its general solution has been given in [27]. Explicitly, taking a modified Laplace transformation $U(z) = \int_{t_0}^\infty u(t, t_0) e^{izt} dt$ to Eq. (11), we have

$$U(z) = \frac{i}{z - \omega_c + i\kappa - \Sigma(z)}. \quad (21)$$

Here, $\Sigma(z) = \int_0^\infty \frac{d\omega}{2\pi} \frac{J_s(\omega)}{z - \omega}$ is the self-energy correction. Furthermore,

$$\lim_{z \rightarrow \omega \pm i\epsilon} \Sigma(z) = \Delta(\omega) \mp \frac{i}{2} J_s(\omega). \quad (22)$$

The principal value $\Delta(\omega) = \sum_\alpha \mathcal{P} \int_0^\infty \frac{d\omega'}{2\pi} \frac{J_\alpha(\omega')}{\omega - \omega'}$ is the cavity frequency shift arisen from the spin ensemble. The general solution of $u(t, t_0)$ is expressed as [27]

$$\begin{aligned} u(t, t_0) &= \sum_{\omega_b} \mathcal{Z}(\omega_b) e^{-i\omega_b(t-t_0)} \\ &+ \int_0^\infty \frac{d\omega}{2\pi} \frac{J_s(\omega) e^{-i\omega(t-t_0)}}{[\omega - \omega_c - \Delta(\omega) + i\kappa]^2 + J_s^2(\omega)/4}. \end{aligned} \quad (23)$$

The first term is the contribution of localized modes, in which the residue $\mathcal{Z}_{\omega_b} = \frac{1}{1 - \Sigma'(\omega_b)}$ is the corresponding bound-state amplitudes. A localized mode can exist if and only if both

conditions are simultaneously satisfied [27]

$$\sum_\alpha J_\alpha(\omega_b) = 0, \quad \omega_b = \omega_c + \Delta(\omega_b). \quad (24)$$

As we show in general non-Markovian dynamics of open quantum systems [27] and also explored in the non-Markovianity measure through two-time correlation functions [38], localized modes are dissipationless and represent a long-time non-Markovian memory effect. The second term in Eq. (23) is a contribution from the branch cut due to the discontinuity of $\Sigma(z)$, so does $U(z)$, across the real axis on the complex space z in the inverse Laplace transformation of Eq. (21). This branch cut usually induces a nonexponential decay which represents a short-time non-Markovian memory effect.

The non-Markovian memory feature can be described more precisely through the noise correlation. In terms of Langevin equation, the color noise (i.e., the memory process or non-Markovian process) is defined by the noise force characterized by $\langle \xi(t) \rangle = 0$ and $\langle \xi(t) \xi(\tau) \rangle = \tilde{g}(t - \tau)$. Here, $\xi(t)$ is given by Eq. (17) and $\tilde{g}(t - \tau)$ is given by Eq. (9b). Using the linear response theory, one can derive the fluctuation-dissipation theorem from the Langevin equation [48]. For a memoryless process, the noise force is δ correlated, i.e., $\langle \xi(t) \xi(\tau) \rangle \propto \delta(t - \tau)$, and its Fourier transform is frequency independent, which is defined as Markovian process. This is not the case for the hybrid system considered in this work. The noise correlation (20) is indeed the nonequilibrium extension of the fluctuation-dissipation theorem in the time domain [27]. Let us take the steady-state limit of the noise correlation $v(t, t + \tau) = \langle \zeta^\dagger(t + \tau) \zeta(t) \rangle$ of Eq. (20), which is the quantity truly characterizing memory processes, i.e., non-Markovian dynamics [38,41,49]. For simplicity, let $\kappa = 0$ in Eq. (23), we have

$$\begin{aligned} v(t, t + \tau) &\stackrel{t \rightarrow \infty}{=} \int_0^\infty \frac{d\omega}{2\pi} \bar{n}(\omega, T) J(\omega) e^{i\omega\tau} \\ &\times \left[\sum_{\omega_b, \omega_b'} \frac{\mathcal{Z}(\omega_b) \mathcal{Z}(\omega_b') e^{-i(\omega_b - \omega_b')t}}{(\omega - \omega_b)(\omega - \omega_b')} \right. \\ &\left. + \frac{1}{[\omega - \omega_c - \Delta(\omega)]^2 + J^2(\omega)/4} \right]. \end{aligned} \quad (25)$$

The frequency dependence of the above noise correlation is the manifestation of color noise as memory or non-Markovianity. The first term and the second term of Eq. (25) are, respectively, the localized mode contribution and the branch cut contribution. The first term is preserved at $\tau \rightarrow \infty$, which indicates that the memory induced by localized modes is a long-time non-Markovian memory effect. The branch cut contribution vanishes at $\tau \rightarrow \infty$ so that it leads to a short-time non-Markovian effect. This is the general picture of non-Markovianity that can be directly measured in experiments through the two-time correlation functions [38]. Note that thermal fluctuation $\bar{n}(\omega, T)$ can also modify non-Markovian memory effect in the low-temperature regime, as shown in Eq. (25).

To see further the long-time memory effect arisen from localized modes, we consider the exact solution of the master

equation (6) for an arbitrary initial state of the cavity system $\rho_c(t_0) = \sum_{l,m=0}^{\infty} \rho_{lm}(t_0) |l\rangle\langle m|$ in the absence of the deriving field $f(t) = 0$. The result has been obtained previously [49],

$$\rho_c(t) = \sum_{l,m=0}^{\infty} \rho_{lm}(t_0) \sum_{k=0}^{\min(l,m)} d_k A_{lk}^+(t) \tilde{\rho}[v(t,t)] A_{mk}(t), \quad (26a)$$

where

$$\tilde{\rho}[v(t,t)] = \sum_{n=0}^{\infty} \frac{[v(t,t)]^n}{[1+v(t,t)]^n} |n\rangle\langle n|, \quad (26b)$$

$$A_{lk}^+(t) = \frac{\sqrt{l!}}{(l-k)! \sqrt{k!}} \left[\frac{u(t,t_0)}{1+v(t,t)} a^+ \right]^{l-k}, \quad (26c)$$

and $d_k = [1 - \frac{u(t,t_0)}{1+v(t,t)}]^{l-k}$. If there is no localized mode, Eq. (23) leads to $u(t \rightarrow \infty, t_0) = 0$. Then, $\rho_c(t \rightarrow \infty) = \lim_{t \rightarrow \infty} \tilde{\rho}[v(t,t)]$ which is a thermal-like state and is independent of the initial cavity state. In other words, the branch cut contribution in Eq. (23) only induces a short-time memory effect, i.e., the initial state information is completely lost after a certain period of time. However, when localized modes exist, $u(t \rightarrow \infty, t_0) = \lim_{t \rightarrow \infty} \sum_{\omega_b} \mathcal{Z}(\omega_b) e^{-i\omega_b(t-t_0)}$ which does not vanish. Consequently, $\rho_c(t \rightarrow \infty)$ always remain some information on the initial cavity state $\rho_{lm}(t_0)$ [see Eq. (26a)], i.e., the state always keeps the memory on initial state information. This shows explicitly how localized modes induce the long-time non-Markovian memory effect.

Furthermore, the long-time memory feature can be understood deeply from the bound-state structure of localized modes. Consider a simple initial state: $|\psi(t_0)\rangle = a^\dagger |0, \{0_k\}\rangle$, i.e., the system is initially in a single-excitation state, and the spin ensemble is in the vacuum so that the Schrödinger equation can be used to determine the evolution of the total system in this special case. By solving exactly the time-dependent Schrödinger equation, the state of the total system at a later time t is given by

$$|\psi(t)\rangle = u(t, t_0) |1_s, \{0_k\}\rangle + \sum_k \alpha_k(t, t_0) |0_s, \{1_k\}\rangle, \quad (27)$$

where $u(t, t_0)$ is determined by Eq. (23) and the coefficient $\alpha_k(t, t_0)$ is given by

$$\alpha_k(t, t_0) = -iV_k \int_{t_0}^t d\tau e^{-i\omega_k(t-\tau)} u(\tau, t_0). \quad (28)$$

Substituting the solution of Eq. (23) into the above relations, we obtain

$$|\psi(t)\rangle \stackrel{t \rightarrow \infty}{\equiv} \left[\sum_{\omega_b} e^{-i\omega_b(t-t_0)} \mathcal{Z}(\omega_b) \left(a^\dagger + \sum_k \frac{V_k}{\omega_b - \omega_k} b_k^\dagger \right) + \sum_k \frac{e^{-i\omega_k(t-t_0)}}{[\omega_k - \omega_s - \Delta(k)] + iJ(k)/2} b_k^\dagger \right] |0, \{0_k\}\rangle. \quad (29)$$

The first term in the above solution is the bound state of a localized mode, which is a highly collective quasiparticle state coherently combining the system and the environmental

modes together:

$$|B(\omega_b)\rangle = \mathcal{Z}(\omega_b) \left(a^\dagger + \sum_k \frac{V_k}{\omega_b - \omega_k} b_k^\dagger \right) |0, \{0_k\}\rangle, \quad (30)$$

where $\mathcal{Z}(\omega_b)$ is the wave-function amplitude of the bound states as shown in Eq. (23). The second term corresponds to the branch cut contribution and will decay (relax) to the vacuum state in the long-time limit. Thus, any change of the environment or the change of the coupling between the system and the environment will response on the structure of the localized bound state. This shows how the non-Markovian memories can be presented for long time through the correlations between the system and environment if localized modes are formed because the system and the environment are coherently correlated forever in the localized bound states. This provides the underlying picture of the long-time non-Markovian memory dynamics induced by the localized bound states.

Of course, it must be pointed out that the description with the Schrödinger equation alone is incomplete for the cavity decoherence dynamics when the spin ensemble is initially in a thermal state (at finite temperature). This is because the thermal state is a mixed state so that the Schrödinger equation is not applicable, and quantum and thermal fluctuations must be taken into account simultaneously through the fluctuation-dissipation theorem. As we have shown, the above solution of the localized bound states remains the same structure in the Green function formulation. Nevertheless, the discussions given in this section show that the non-Markovian memory dynamics is a manifestation of dissipation and fluctuation dynamics together, which provide a rather complete physical picture on decoherence dynamics for open quantum systems in the framework of the exact master equation.

III. DECOHERENCE DYNAMICS OF THE CAVITY COUPLED STRONGLY TO THE SPIN ENSEMBLE

Based on the general non-Markovian decoherence theory presented in the last section, we take applications to the realistic hybrid quantum systems in the this and the next sections. In the two recent experimental setups by Putz *et al.* [29,30], the superconducting microwave cavity frequency ω_c is set to $2\pi \times 2.69$ GHz, and the main frequency ω_s of the spin spectral density is resonant with the cavity $\omega_s = \omega_c$, but has the broadening effect. Also, spins are surrounded by a Helmholtz coil which supplies a strong magnetic field to modify the spins into the polarized ground state. To reduce the thermal fluctuation effect, the entire experimental setup is cooled down to $T = 25$ mK, which is only about one-fifth of the excitation energy of spins. By applying a driving field, the cavity photonic state may be coherently stored and retrieved from the spin ensemble for quantum information processing. By controlling the strength of the driving pulse, the number of injected photons is manifested to be about or less than 10^6 , which is much lower than the total number of spins $\approx 10^{12}$ in the cavity so that the Holstein-Primakoff approximation to the spin ensemble is valid.

The main difference in the two experiments of Refs. [29] and [30] is the manipulation of the broadening spectral density

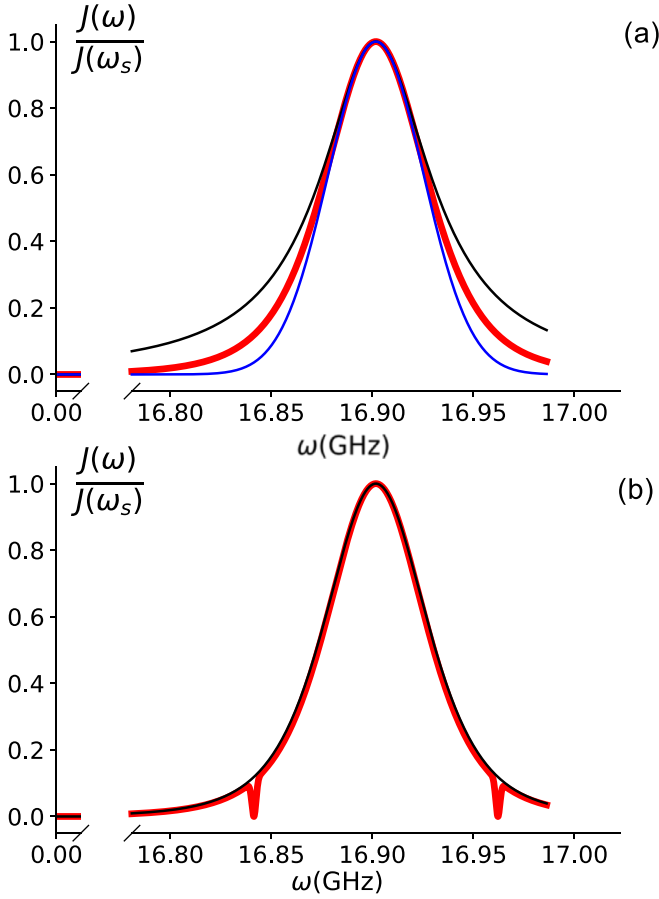


FIG. 1. The spectral density $J(\omega)$ of the spin ensemble, Eq. (31), as a function of the frequency. (a) The black, blue, and red curves correspond to the spectral densities of a Lorentzian form ($q = 2$), a Gaussian form ($q = 1$), and the q -Gaussian form ($q = 1.39$), respectively. (b) The black (thin) curve is the original q -Gaussian form ($q = 1.39$), and the red (thick) curve is modified from the q -Gaussian form by the hole-burning technique [30]. Here, the tendency of $J(\omega) \rightarrow 0$ as $\omega \rightarrow 0$ is also shown.

of the spin ensemble. The spectral density of Eq. (10a) is experimentally fitted as a q -Gaussian spectral density [29]

$$J(\omega) \equiv J_s(\omega) = 2\pi\Omega^2\rho(\omega) = 2\pi\Omega^2C \left[1 - (1-q)\frac{(\omega - \omega_s)^2}{\Delta^2} \right]^{\frac{1}{1-q}}, \quad (31)$$

with $q = 1.39$, which is an intermediate form between a Gaussian spectral density ($q = 1$) and a Lorentzian spectral density ($q = 2$). Here, C is its normalization constant $\int d\omega \rho(\omega) = 1$, ω_s is the main frequency of the spin ensemble, Δ is determined by the full width at the half-maximum of $J(\omega)$ which is given by $\gamma = 2\Delta\sqrt{\frac{2^q-2}{2q-2}} = 18.8\pi$ MHz. The coupling strength $2\Omega = 2\pi \times 17.2$ MHz represents a strong coupling in Ref. [29]. The specific profile of the spectral density $J(\omega)$ is shown in Fig. 1(a). While the spectral density in another experiment [30] is a modification of Eq. (31) as shown in Fig. 1(b), which is made by the spectral hole-burning technique, a well-established technique in quantum optics used to turn off the excitations at some specific frequencies in

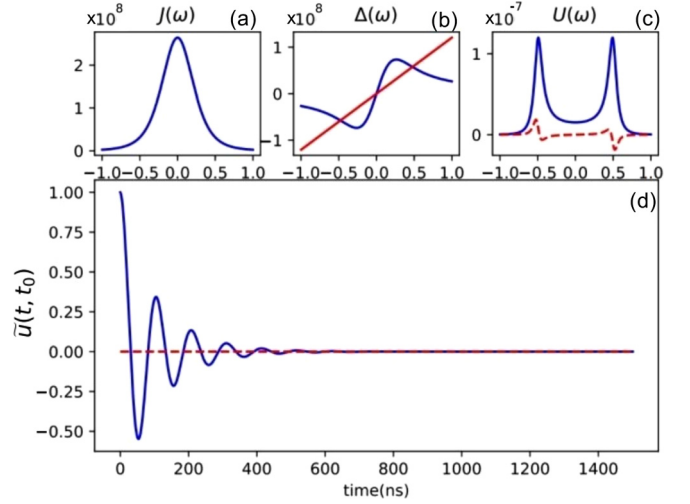


FIG. 2. (a) The q -Gaussian spectral density $J(\omega)$ (in units of Hz for $\hbar = 1$) with respect to the frequency ω in the units of Ω_R (after a central frequency shift $\omega - \omega_s \rightarrow \omega$, where $\omega_s = \omega_c$), which is also proportional to the imaginary part of the self-energy. (b) The blue curve is the real part of the self-energy (in units of Hz), the crossing points with the red line are the solution of $\Delta(\omega) = \omega$. (c) The blue (real) and red (dot) curves are the real and imaginary parts of $U(\omega)$ (in units of 1/Hz), respectively. Note that (a)–(c) solved from the Fourier transformation of Green function $u(t, t_0)$. (d) The inverse Laplace transformation of $U(\omega)$, i.e., the solution of Green function $u(t, t_0)$ which is dimensionless. The blue (real) and the red (dot) curves correspond to the real and imaginary parts of $\bar{u}(t, t_0) \equiv u(t, t_0)e^{i\omega_c(t-t_0)}$ with $t_0 = 0$.

the spin ensemble. Here, the particular frequencies of $\omega_s \pm \frac{\Omega_R}{2}$ are burnt out as shown in Fig. 1(b). Besides, in the experiment [30], the full width at half-maximum of the spectral density is changed slightly to 18.2π MHz, and the coupling strength $\Omega \approx \frac{\Omega_R}{2} = 21.3\pi$ MHz with Ω_R being the Rabi frequency. The cavity decay rate $\kappa/2\pi = 0.4$ MHz counting the leakage effect. Our calculations are all based on these experimental parameter setups. We set $\hbar = 1$ hereafter so that the energy has the same unit as frequency.

For the spin ensemble with the q -Gaussian spectral density, Eq. (31), the central frequency $\omega_s = 2\pi \times 2.69$ GHz which is much larger than the spectral width $\gamma = 18.8\pi$ MHz. Thus, the spectral density at $\omega = 0$ is nearly zero, i.e., $J(0) \simeq 0$ as shown in Fig. 1. From Figs. 2(a) and 2(b), we see that even though $J(\omega) \simeq 0$ for $\omega \leq 0$, another localized mode condition in Eq. (24), $\omega_b = \omega_c + \Delta(\omega_b)$ cannot be satisfied [see Fig. 2(b)] so that no localized bound state can exist for $\omega \leq 0$. As a result, the solution (23) for $u(t, t_0)$ is simply reduced by

$$u(t, t_0) = \frac{2}{\pi} \int_0^\infty d\omega \frac{J(\omega)e^{-i\omega(t-t_0)}}{4[\omega - \omega_c - \Delta(\omega) + i\kappa]^2 + J^2(\omega)}. \quad (32)$$

Figures 2(c) and 2(d) present all the decoherence information of the cavity system. These results are independent of the specific initial state of the cavity one takes.

Experimentally, the photon number is measured by detecting the transmission intensity of the cavity field. Our theory

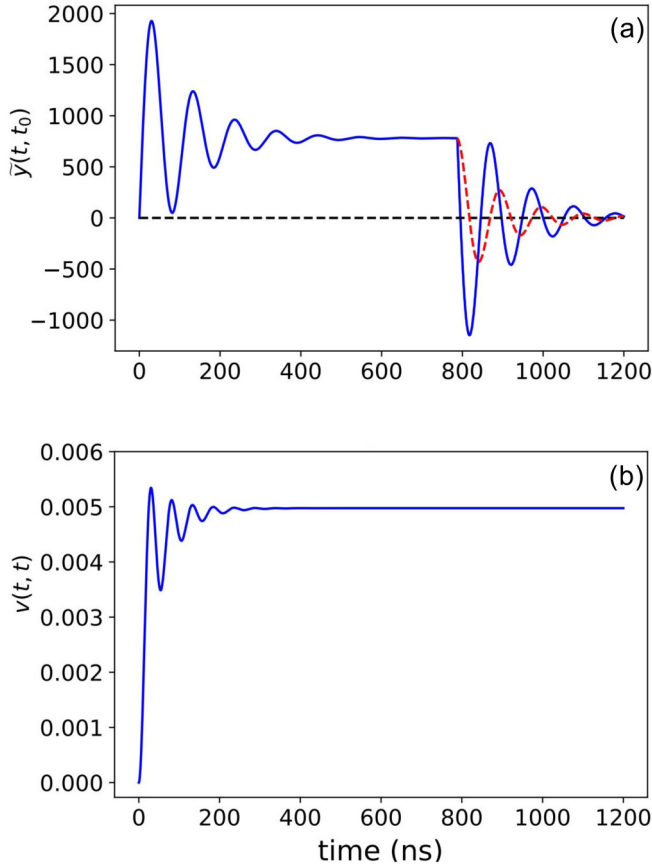


FIG. 3. (a) The blue line is the evolution of cavity response field $\tilde{y}(t, t_0) = y(t, t_0)e^{i\omega_c t}$ with respect to a rectangular driving field at the resonant frequency $\omega_p = \omega_c = \omega_s$, the damping is caused by the spin ensemble for the q -Gaussian spectral density. The red dashed line is given by Eq. (35) for the time duration $t \geq t_{\text{off}}$. (b) The photon fluctuation $v(t, t)$ of Eq. (12b) induced by spin ensemble at temperature $T = 25$ mK, which is negligible in comparison with the driving-field-induced cavity field $|y(t, t_0)|^2$, as shown in the figure. Both $\tilde{y}(t, t_0)$ and $v(t, t)$ are dimensionless.

gives the solution to the cavity photon number, i.e., Eq. (13b), which is divided into four terms. The first term represents the dissipation of the initial photons in the cavity. The second term is the cavity response to the driving field. The third term shows the photon fluctuations induced by the spin ensemble and the environment. The last term is the interference between the initial cavity photons and the driving field response photons. In the experiment [29], the cavity system is initially set in the vacuum. Hence, the first and the last terms vanish in Eq. (13b) so that the cavity intensity is simply reduced to

$$\langle n(t) \rangle = |y(t, t_0)|^2 + v(t, t), \quad (33)$$

where $y(t, t_0)$ and $v(t, t)$ are given by Eq. (12) which is determined by the solution of Eq. (32).

The solutions of $y(t, t_0)$ and $v(t, t)$ are plotted in Fig. 3 in which $\tilde{y}(t, t_0) = y(t, t_0)e^{i\omega_c(t-t_0)}$. It shows that the cavity response field undergoes two damping processes. The first damping takes place when a rectangular driving field is applied to the cavity. The cavity photons are raised up to the maximum very quickly. In the meantime they are dissi-

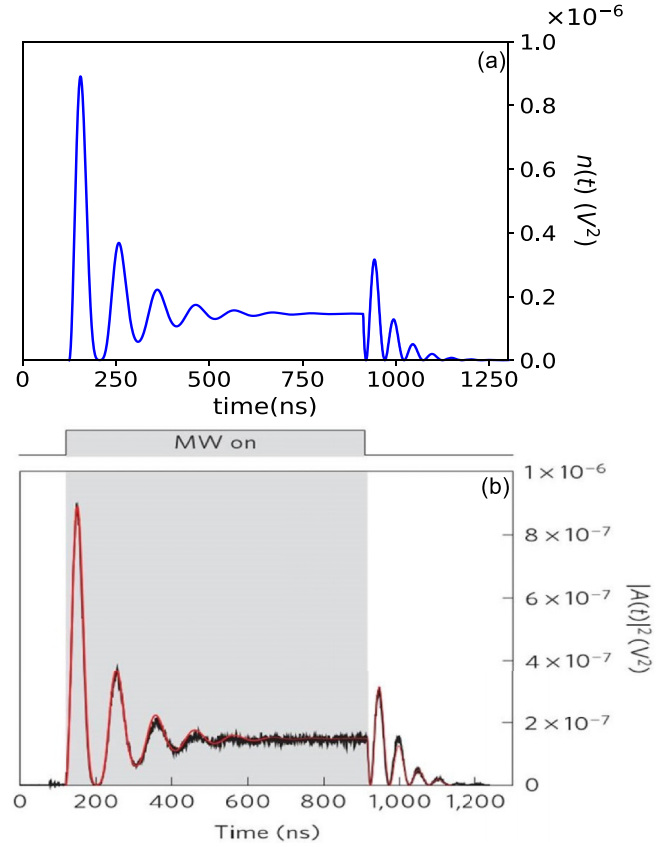


FIG. 4. (a) The cavity intensity under a rectangular driving field calculated from our theory. (b) The cavity intensity measured (black curve) in experiment and the semiclassical description (red curve) given in Fig. 2(b) of Ref. [29]. The cavity intensity has been converted to electric signal in unit of V^2 as shown in experiment.

pated into the spin ensemble which is described in Eq. (12a) through the Green function $u(t, t_0)$; the corresponding oscillating damping is similarly shown in Fig. 2(d). The decay lasts a certain time t_s ($t_s < 600$ ns for the parameters given in [29]), and the cavity photons gradually reach a saturation, i.e., $y(t_s, t_0) \simeq y(t_{\text{off}}) = \langle a^\dagger(t_{\text{off}}) \rangle$ after $t_s \simeq 600$ ns. Also note that the oscillating damping is the manifestation of a short-time non-Markovian cavity decoherence induced by the inhomogeneous broadening of the spin ensemble spectrum, as we will discuss in details later.

After the driving field is turned off at the time t_{off} , the cavity field undergoes the second damping, as shown by the blue solid line in Fig. 3(a). This result is directly obtained from the solution of $y(t_{\text{off}} + \tau, t_0)$ which can be reduced to

$$\tilde{y}(t_{\text{off}} + \tau, t_0) = \tilde{y}(t_{\text{off}}) - \tilde{y}(\tau, t_0), \quad (34)$$

which shows that the second damping process is off phase with the first damping process. As a result, the timescale of the second damping in the observation of the cavity intensity is only a half of the decay time of the first damping, as shown in Fig. 4. On the other hand, the second damping process contains two parts, one is the restarted damping of the cavity response field $y(t_{\text{off}})$ after the driving field is turned off, which

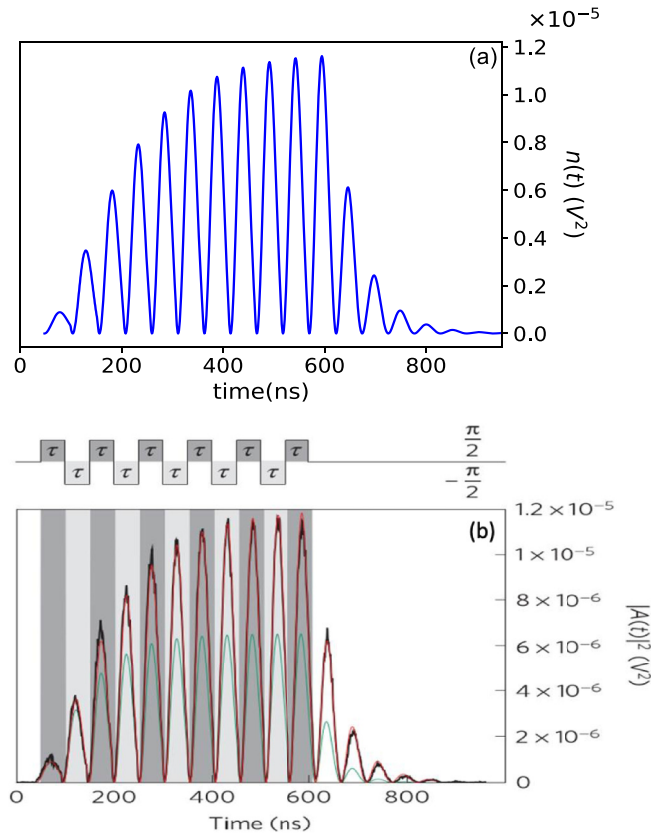


FIG. 5. (a) The cavity intensity under a phase-shifting driving field calculated from our theory, similar to the plot of Fig. 4. (b) The cavity intensity measured (black curve) in experiment and the semiclassical description (red curve), as shown in Fig. 4(b) of Ref. [29].

is given by

$$\tilde{y}_1(t_{\text{off}} + \tau, t_0) = \tilde{u}(\tau, t_{\text{off}})\tilde{y}(t_{\text{off}}). \quad (35)$$

The result is shown by the red dashed line in Fig. 3(a). The difference between the blue solid line and the red dashed line in Fig. 3(a) is the field retrieved back from the spin ensemble, regarded usually as the quantum memory in hybrid quantum systems [29].

With the above detailed picture how the cavity response to the driving field is decohered into the spin ensemble and how it is retrieved back from the spin ensemble after the driving field is turned off, we present in Figs. 4 and 5 the cavity intensity of Eq. (33) with a rectangular driving field and a π -phase-shifting driving field, respectively, in a comparison with the experiment observations at the same conditions [29]. Figures 4(a) and 5(a) show that our theoretical solutions are in good agreement with the experimental data of Figs. 4(b) and 5(b) [corresponding to Figs. 2(b) and 4(b) in Ref. [29]]. In fact, the authors of Ref. [29] used a semiclassical approach (the Volterra integral equation) to describe the cavity photon dynamics, and their results [see the red curves in Figs. 4(b) and 5(b)] also fitted the experimental data very well, also see [32]. This is because the driving field is a classical field containing photon number ($\approx 10^6$) and the temperature is set to be very low (≈ 25 mK $\sim \frac{1}{5}\hbar\omega_c$) in the experiment. The corresponding photon fluctuations given by $v(t, t)$ are indeed very

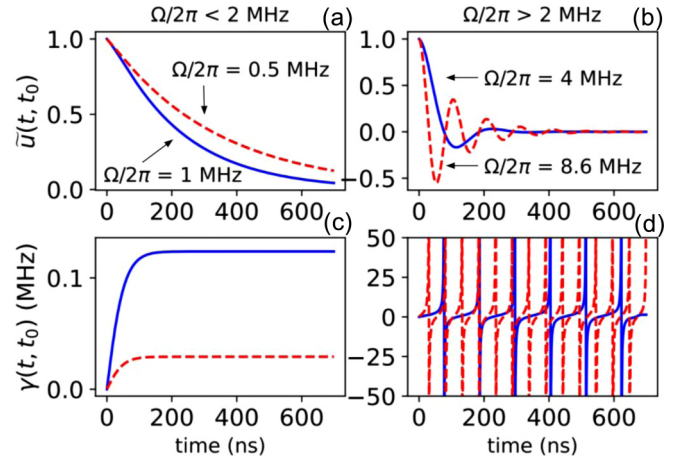


FIG. 6. Decoherence dynamics of the cavity photons dissipating into the spin ensemble for different coupling strength Ω between the cavity and the spin ensemble; the same other parameters are taken as given in the experiment [29]. (a), (b) The time evolution of the Green function $u(t, t_0)$ for the coupling strength $\Omega/2\pi = 0.5, 1.0$ MHz and 4, 8.6 MHz, respectively. (c), (d) The corresponding dissipation coefficient $\gamma(t, t_0)$ determined by Eq. (36).

very small, namely, $v(t, t) \ll |y(t, t_0)|^2$, as shown in Fig. 3 [comparing the magnitude difference between Figs. 3(a) and 3(b)]. This gives the reason why the semiclassical approach used in [29] can fit very well with the experimental data.

On the other hand, the oscillating damping in Figs. 4 and 5 manifest the non-Markovian decoherence dynamics of the cavity field induced by the spin ensemble, here the cavity leakage is very small ($\kappa = 2\pi \times 0.4$ MHz $\ll \Omega = 2\pi \times 8.6$ MHz) [29]. These oscillating dampings can be characterized by the dissipation coefficient $\gamma(t, t_0)$ in the exact master equation (6) and can be explicitly computed through Eq. (7a) which is again determined by the Green function $u(t, t_0)$ of Eq. (32):

$$\gamma(t, t_0) = -\text{Re}[\dot{u}(t, t_0)/u(t, t_0)]. \quad (36)$$

Some results are plotted in Fig. 6. Taking the same parameters used in experiment [29], we find that when the coupling strength $\Omega/2\pi < 2$ MHz (weak couplings), the Green function $u(t, t_0)$ shows an exponential decay [see Fig. 6(a)], which is the Markovian decoherence process. The corresponding decay rate is given by the asymptotic value of $\gamma(t, t_0)$ [see Fig. 6(c)]. The asymptotic value is $\gamma(t \rightarrow \infty, t_0) \simeq 2\kappa + J(\omega_s)$, as expected in the experiment observation in [29].

For the strong coupling (here $\Omega/2\pi > 2$ MHz), the decoherence dynamics is very different. The Green function $u(t, t_0)$ is no longer a simple exponential decay, it involves an oscillating damping for the cavity field as shown in Fig. 6(b). Such oscillating damping leads to the stronger oscillation of the dissipation coefficient $\gamma(t, t_0)$ in time, as shown in Fig. 6(d). As it is well known, the oscillation of dissipation coefficient between positive and negative values is the evidence of non-Markovian decoherence dynamics. In particular, the sudden change in the dissipation coefficient from a huge positive value to a huge negative value corresponds to forward and backward rapid photon (and information) flows between the cavity and the spin ensemble in a rather short time. As

the coupling becomes stronger and stronger, such forward and backward rapid photon flows get faster and faster. This is a direct and significant manifestation of non-Markovian dynamics.

To understand further the above non-Markovian decoherence feature induced by the spin ensemble, we take the Lorentzian spectral density as a comparison. For the Lorentzian spectral density, $J(\omega) = 2\Omega^2 \frac{\Delta}{(\omega - \omega_c)^2 + \Delta^2}$, i.e., Eq. (31) with $q = 2$, the Green function $u(t, t_0)$ can be analytically solved:

$$u(t, t_0) = \exp \left\{ - \left(i\omega_c + \frac{\Delta}{2} \right) (t - t_0) \right\} \times \left(\cosh \frac{\Delta'(t - t_0)}{2} + \frac{\Delta}{\Delta'} \sinh \frac{\Delta'(t - t_0)}{2} \right), \quad (37)$$

where $\Delta' = \sqrt{\Delta^2 - 4\Omega^2}$. It is well known that the Markovian and non-Markovian dynamics occur in the weak- and strong-coupling regimes $\Omega < \Delta/2$ and $\Omega > \Delta/2$, respectively, with $\Omega = \Delta/2$ being the transition point [27,50,51].

For the weak coupling $\Omega < \Delta/2$, Eq. (37) shows that the cavity field mixes two decay processes with decay rates $\Gamma_{\pm} = \Delta \pm \Delta'$,

$$\tilde{u}(t, t_0) = \frac{1}{2} \left(1 + \frac{\Delta}{\Delta'} \right) \exp \left\{ \frac{1}{2} (\Delta - \Delta') (t - t_0) \right\} + \frac{1}{2} \left(1 - \frac{\Delta}{\Delta'} \right) \exp \left\{ -\frac{1}{2} (\Delta + \Delta') (t - t_0) \right\}, \quad (38)$$

where $u(t, t_0) \equiv \tilde{u}(t, t_0) e^{-i\omega_c(t-t_0)}$. As we can see, both terms in Eq. (38) show exponential decays with different decay constants $\Delta \mp \Delta'$, which lead to a positive-definite decay coefficient $\gamma(t, t_0)$ in time, as a criterion for Markovianity [51]. It also shows that the small-amplitude part (the second term) decays faster (mainly happening in short time) and the large-amplitude part (the first term) decays slower (lasting longer), as the coupling increases. The overall effect shows that the damping becomes stronger as the coupling increases.

For the strong coupling $\Omega > \Delta/2$, the cavity field damping is analytically described by

$$\tilde{u}(t, t_0) = \frac{1}{2} \left[\left(1 - \frac{\Delta}{\omega'} \right) e^{i\omega'(t-t_0)} + \left(1 + \frac{\Delta}{\omega'} \right) e^{-i\omega'(t-t_0)} \right] \times \exp \left\{ -\frac{\Delta}{2} (t - t_0) \right\}, \quad (39)$$

where $\omega' = \sqrt{4\Omega^2 - \Delta^2}$. It shows that the decay factor is a simple exponential decay but the field amplitude strongly oscillates as the coupling increases. This leads to the rapid oscillation of the dissipation coefficient $\gamma(t, t_0)$ between positive and negative values in time, similar to the situation shown in Fig. 6(d) for spin ensemble. This is the evidence of manifesting non-Markovian decoherence dynamics, even though the whole amplitude profile decays exponentially with a constant decay rate $\Gamma = \Delta$ (note that a pure exponential decay without amplitude oscillations corresponds to a Markovian process).

The rapidly oscillating dissipation coefficient $\gamma(t, t_0)$ between positive and negative values in time is the clear signature for non-Markovian dynamics, manifested through the rapidly forward and backward information flow between

the cavity and the reservoir. It is interesting to see whether such a rapid information flow plays a similar role as dynamical decoupling through a rapid time-dependent control modulation (spin echo) for decoherence suppression [52,53], even though the mechanisms are completely different. The former comes from the symmetric spectral density where the spectral density is the decoherence source, while the latter is generated from the external control pulses. The analytical solution for the Lorentzian spectral density shows that the decay rate for the whole amplitude profile retains a constant as the coupling increases, which seems to have no decoherence suppression in the strong-coupling regime [19]. But by comparing to the decay dynamics in the weak-coupling regime, we see that the dominated decay process [the first term in Eq. (38)] is enhanced as the coupling increases (because $\Delta - \Delta'$ increases as Ω increases). Thus, the decay rate retains a constant (i.e., no increase) as Ω increases in the strong-coupling regime for the Lorentzian spectral density may be considered as a modest suppression of decoherence. In this sense, the rapidly forward and backward information flow for the non-Markovian dynamics in the strong coupling provides the qualitative picture how the decoherence is suppressed in the strong coupling, comparing with the decoherence in the weak-coupling regime. Such decoherence suppression becomes more significant for the q -Gaussian spectral density of Eq. (31), a deformed Lorentzian spectral density, as observed [29].

For a more intuitive understanding, we plot the decoherence dynamics in Fig. 7 for the Lorentzian spectral density and the Gaussian spectral density similar to that plotted in Fig. 6. The results show that in the weak-coupling regime, the decay is enhanced as the coupling increases for all three spectral densities, but the strongest enhancement is Gaussian spectral density, then the q -Gaussian, and then Lorentzian, as shown from the steady-state values of the decay coefficients plotted in Figs. 6(c), 7(c) and 7(g). On the contrary, for strong coupling, the decay of all three spectral densities is suppressed, but the suppression is modest for Lorentzian, then becomes strong for q -Gaussian, and stronger for Gaussian, as shown through the decays of the amplitude profiles plotted in Figs. 6(b), 7(b) and 7(f). This can also be seen from Figs. 6(d), 7(d) and 7(h), where the oscillations of the decay coefficients between the huge positive and negative values become faster and faster from Lorentzian to the q -Gaussian, then to Gaussian, as a manifestation of decoherence suppression. These decoherence suppression behaviors correspond to cavity protection effect studied in [19] but actually it is not the property only for cavities but also for any other open systems with such symmetric spectral densities.

It may also be worth pointing out that for frequency-dependent spectral densities, the corresponding decoherence dynamics cannot be characterized by a single decay constant. This is because for non-Markovian decoherence dynamics, the decay is always time dependent, as characterized by the time-dependent decay coefficient in the exact master equation as well as in the exact quantum Langevin equation. It is the time-dependent decay coefficient that depicts the transient decoherence dynamics (the oscillations) in the real-time domain. The detailed decoherence dynamics is rather sensitive to the spectral density profile [27,49]. The perfect decoherence suppression for the rectangular spectral density studied

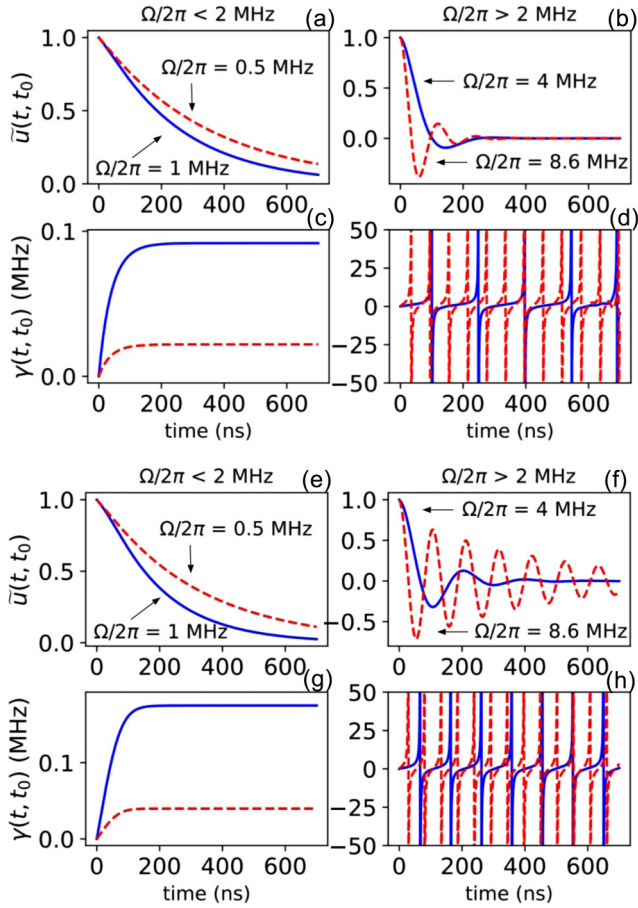


FIG. 7. Decoherence dynamics of the cavity coupled to a spin ensemble in the weak and strong couplings. The top panel is for a Lorentzian spectral density. (a), (b) The time evolution of the Green function $u(t, t_0)$. (c), (d) The corresponding dissipation coefficient $\gamma(t, t_0)$. The bottom panel is for a Gaussian spectral density. (e), (f) The time evolution of the Green function $u(t, t_0)$. (g), (h) The corresponding dissipation coefficient $\gamma(t, t_0)$.

in [19] is indeed arisen from the localized modes, as we have also shown earlier in the tight-binding spectral density [21,22], as well as will be discussed in the next section for the hole-burning spectral density, where the existence of localized bound states provides another physical mechanism for decoherence suppression.

IV. DECOHERENCE SUPPRESSION BY HOLE-BURNING SPECTRA

In another experiment of Putz *et al.* [30], the spectral density of the spin ensemble is modified by the spectral hole-burning technique which was proposed in [33]. The spectral density after hole-burning frequencies at $\omega_s \pm \frac{\Omega_R}{2}$ is shown in Fig. 1(b) [also see Fig. 8(a)]. In Fig. 8(b), the intersection points of the self-energy $\Delta(\omega)$ with the red line are located at frequencies $\omega_s \pm \frac{\Omega_R}{2}$, which result in two localized modes [27] by the conditions: $J(\omega) = 0$ and $\omega - \omega_s - \Delta(\omega) = 0$ of Eq. (24) if the cavity leakage κ can be ignored. The Green

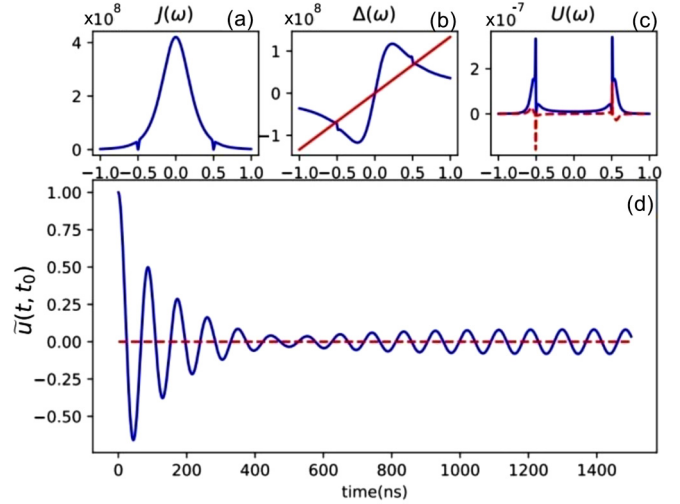


FIG. 8. (a)–(d) The same plot as Fig. 2 but the spectral density has been modified by the spectral hole burning at $\omega = \omega_s \pm \frac{\Omega_R}{2}$.

function $u(t, t_0)$ is then given by

$$u(t - t_0) = \mathcal{Z}(\omega_+) e^{-i\omega_+(t-t_0)} + \mathcal{Z}(\omega_-) e^{-i\omega_-(t-t_0)} + \int_0^\infty \frac{d\omega}{2\pi} \frac{J^h(\omega) e^{-i\omega(t-t_0)}}{[\omega - \omega_c - \Delta(\omega)]^2 + [J^h(\omega)/2]^2} \quad (40)$$

with two localized modes $\omega_\pm = \omega_c \pm \Omega_R/2$. More explicitly, the two localized modes correspond to two bound states

$$|B(\omega_\pm)\rangle = \mathcal{Z}(\omega_\pm) \left(a^\dagger + \Omega \int_0^\infty d\omega \frac{\rho^h(\omega)}{\omega_\pm - \omega} b_\omega^\dagger \right) |0, \{0_\omega\}\rangle, \quad (41)$$

where $J^h(\omega) = 2\pi\Omega^2\rho^h(\omega)$, and $\rho^h(\omega)$ is the hole-burned density of state of the spin ensemble spectrum shown in Fig. 1(b). As one can see, the above bound states are the bound states of collective quasiparticles correlating the origin cavity mode with all different modes in the spin ensemble together through their couplings under the hole-burning modification of the spin ensemble spectrum. These two localized bound states correspond to the hybridized polaritonic states [30,33] observed as the peaks in the spectral transmitted steady-state intensity, as shown in Fig. 4d of Ref. [30]. More specific, putting the first two terms of Eq. (40) together has been called a collective dark state in [30]. The last term in Eq. (40) comes from the branch cut that leads to the cavity field damping, which is called the subradiant states in [30].

It should be pointed out that these localized bound states are not the same as the dark states studied in quantum optics [54]. Here, the wave-function amplitude $\mathcal{Z}(\omega_\pm)$ is fully determined by the spectral density of the broadening spin ensemble incorporating the hole burning. As shown from Eq. (41), each localized bound state can trap all different frequency modes together because of the spectral broadening that the cavity coupled with. But, the above two bound states themselves correspond to two independent quasiparticles and are uncoupled from each other so that no Rabi oscillation occurs between these two localized bound states through the controls of the

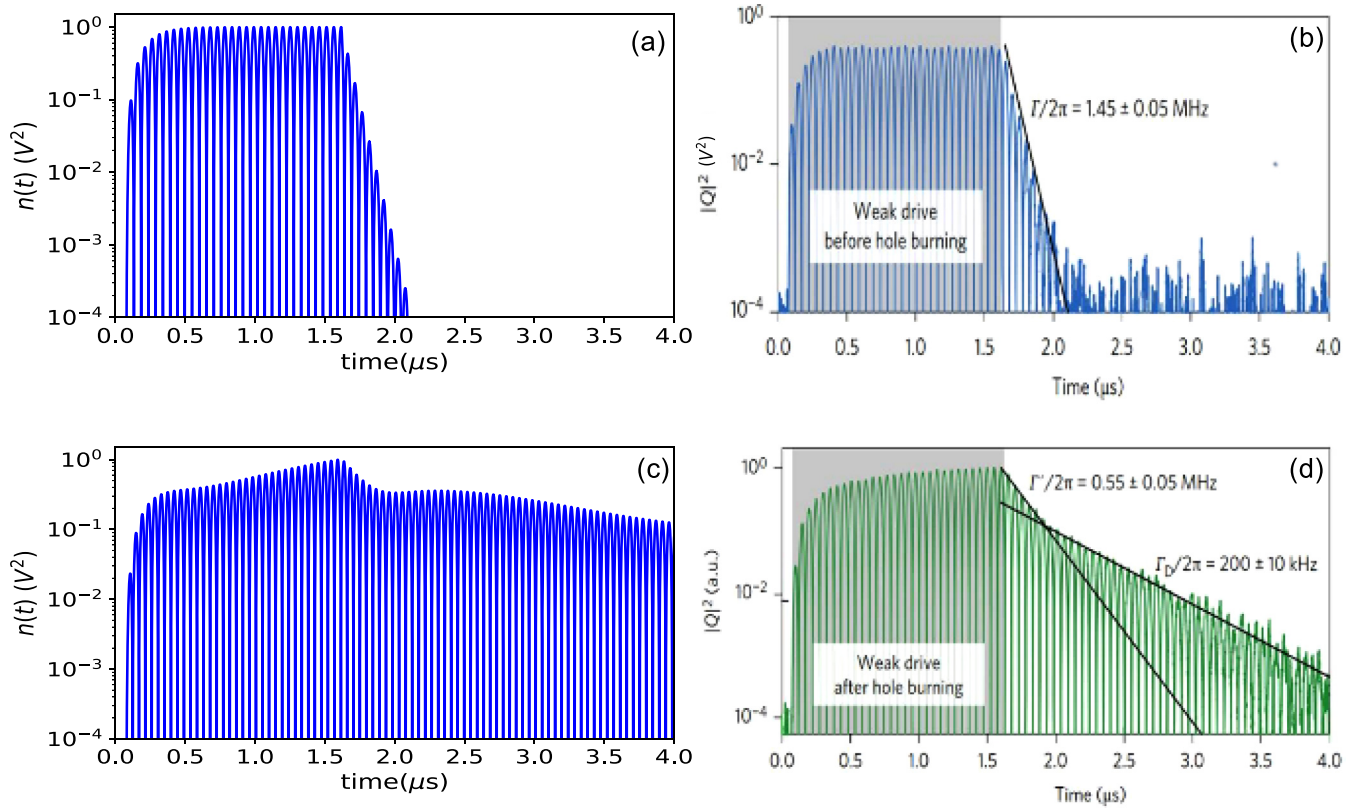


FIG. 9. Cavity intensity for the q -Gaussian spectral density without (a), (b) and with (c), (d) the spectral hole burning, under a sinusoidal driving field, in which (a) and (c) are the theoretical calculations from our theory; (b) and (d) are the experimental measurements by Putz *et al.*, as shown by Figs. 3(e)–3(f) in Ref. [30].

coupling Ω and the driving field $f(t)$, their wave-function amplitudes $\mathcal{Z}(\omega_{\pm})$ are fixed. Thus, it is not easy to retrieve photon states back when the photons are trapped in these localized bound states because these states correlate collectively all possible modes from the spin ensemble. In other words, because localized bound states correlate all possible modes from the spin ensemble, these localized bound states can suppress decoherence but lack the property of the dark states for retrieving information back with high efficiency [54].

The two sharp peaks at $\omega_s \pm \frac{\Omega_R}{2}$ in Fig. 8(c) show the positions of the two localized modes, respectively, located at the hole-burning frequencies in the spectral density. In other words, the hole-burning positions proposed in [33] generate the two special cavity localized bound states discussed above. A similar idea for such decoherence suppression was proposed earlier in [23] but of course the hole-burning technique proposed in [33] is excellent for such a realization of decoherence suppression. As a result, the Green function $u(t, t_0)$ keeps oscillation in time, contributed from these two localized modes, as shown in Fig. 8(d). In other words, the cavity field will not reach a steady state with the spin ensemble, as a dissipationless process (decoherence suppression) arisen from the spectral hole burning. This changes significantly the decoherence dynamics of the cavity field, as observed in [30]. Note that in the ideal case, the peaks in Fig. 8(c) should be δ functions, as the evidence of perfect localized states. However, due to the existence of a small cavity leakage ($\kappa \neq 0$), the

peaks have a small finite width which results the cavity field in a very slow decay in the long time, which is not plotted in Fig. 8(d).

In the experiment [30], the cavity intensity is measured while applying a sinusoidal modulated pulse. Figure 9 shows a comparison of the cavity intensity with and without the spectral hole burning to the spin ensemble spectrum. Both the theoretical calculations and the experimental results show that, without the spectral hole burning, the cavity intensity has an exponential decay (a linear decay in logarithmic timescale) after the driving field is turned off [see Figs. 9(a) and 9(b)]. While, with the spectral hole burning, the cavity damping slows down significantly after the driving field is turned off [see Figs. 9(c) and 9(d)]. In other words, the coherence time is substantially improved. This is the effect of the dissipationless localized modes due to the spectral hole burning on the spin ensemble, as shown in [30].

Also note that the theoretical and the experimental results shown in Figs. 9(c) and 9(d) do not fit each other very well. This is because the decoherence dynamics is rather sensitive to the position and also the shapes of the burning holes. In addition to the spectral hole burning at frequencies given in [30,33], we also consider burning frequencies at different positions to see how the decoherence dynamics of the cavity field sensitively depends on the shape of the spectral density. In Fig. 10(a), the spectrum is burnt at $\omega_s = \omega_c$. Theoretically, there may exist a localized mode at frequency ω_s if the cavity decay κ can be negligible so that the decoherence can be suppressed.

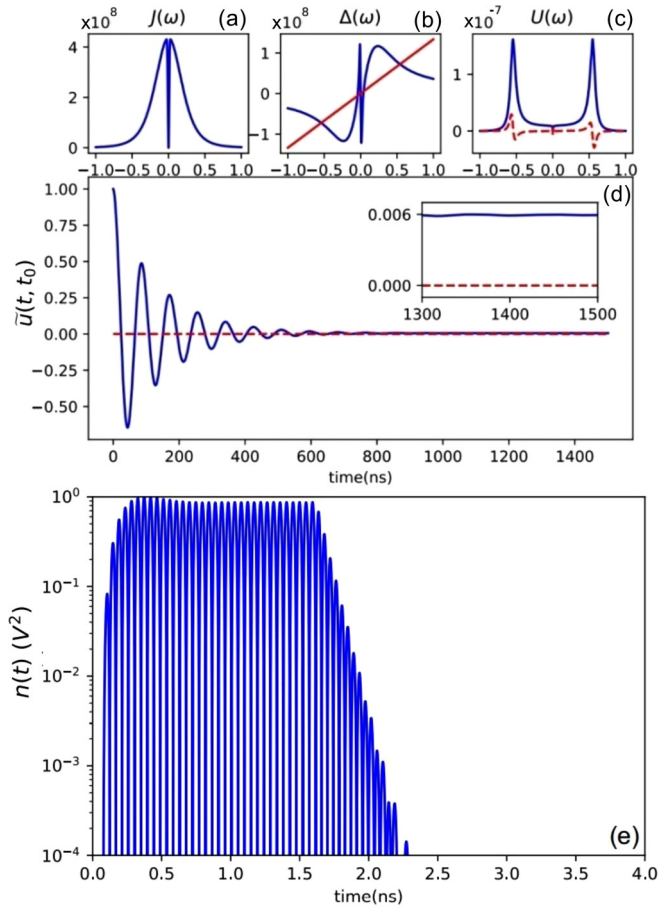


FIG. 10. (a)–(d) The same plot as Fig. 8 with a burning frequency at $\omega = \omega_s$. (e) The corresponding cavity intensity for a sinusoidal driving field.

However, because the slope of $J(\omega)$ at ω_s [see Fig. 10(a)] is so steep such that the amplitude of this localized mode is very very small, as shown by a tiny dip at ω_s in the Fig. 10(c). In other words, the burning frequency almost has no effect on the cavity decoherence dynamics, as shown in the inset of Fig. 10(d). The experimentally observable cavity intensity is plotted in Fig. 10(e) for a sinusoidal driving field. The result is very similar to the solution without the hole burning as shown in Fig. 9(a).

If the spectrum is burnt at $\omega_s \pm \frac{\Omega_R}{4}$ as shown in Fig. 11(b), then the decoherence dynamics also has not much difference in comparing with the case without hole burning [see Figs. 2(d) and 11(d) and also 10(d)], even though the decay is slowed down a little bit. This is because no localized bound state can be generated in this case; the two conditions given by Eq. (24) cannot be simultaneously satisfied. This shows that the burning frequencies must be chosen very close to the position of the intersection points with the red line in Fig. 11(b), i.e., at the half-maximum of the spectral density so that the dissipationless localized modes between the cavity and the spin ensemble can be formed and the wave-function amplitude of these localized bound states can be visibly large. Finally, we examine an example of how much the burning frequency is close to the intersection points $\omega_s \pm \frac{1}{2}\Omega_R$ between the self-energy $\Delta(\omega)$ and the red line in Fig. 8(b) such that

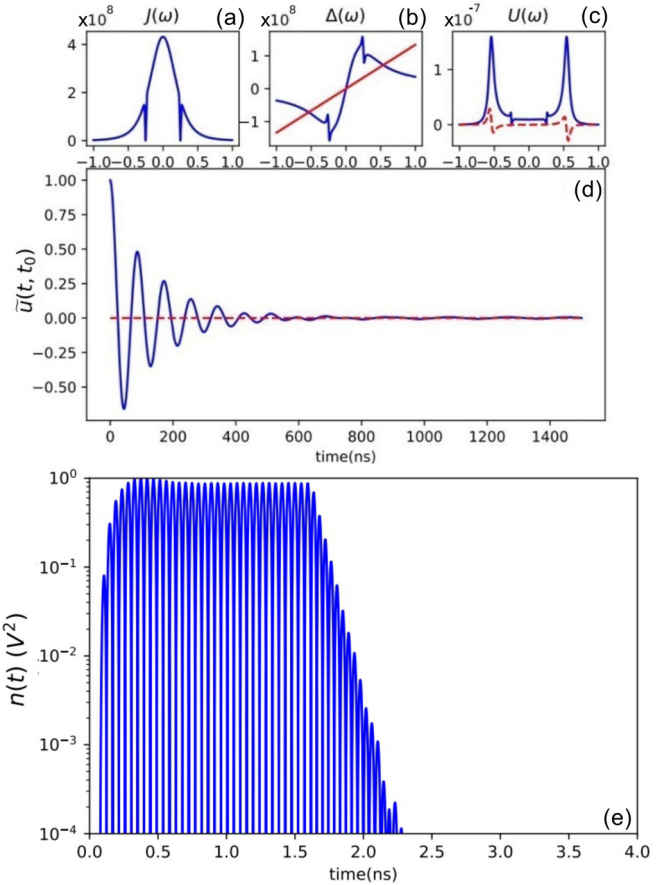


FIG. 11. (a)–(d) The same plot as Fig. 8 with a pair-burning frequency at $\omega = \omega_s \pm \frac{\Omega_R}{4}$. (e) The corresponding cavity intensity for a sinusoidal driving field.

the decoherence can be effectively suppressed. As shown in Fig. 12, when the hole burning is made at $\omega_s \pm (\frac{1}{2} + 0.05)\Omega_R$ (a little bit away from the intersection points $\omega_s \pm \frac{1}{2}\Omega_R$), the decoherence suppression is significantly reduced. We further find that the visible decoherence suppression by hole burning shows up only in the very narrow windows $\omega_s + (\frac{1}{2} \pm 0.1)\Omega_R$ and $\omega_s - (\frac{1}{2} \pm 0.1)\Omega_R$. No suppression effect can be seen outside of the above windows because no localized bound state can be effectively formed. These detailed analyses show that the hole-burning spectral density at the right positions generates localized modes. These localized modes correspond to collective bound states of the cavity entangled with all possible modes in the spin ensemble that can largely suppress the cavity decoherence.

V. CHARACTERIZING QUANTUM MEMORY WITH TWO-TIME CORRELATION FUNCTIONS

The above two sections provide a rather complete description of dissipation (decay) dynamics of the hybrid quantum system that has been experimentally measured. As it is shown, the dissipation dynamics is determined by the Green function $u(t, t_0)$, from which we find how the driving-field-induced cavity response field $y(t, t_0)$ changes in time through Eq. (12). It depicts the information of cavity state decays induced by

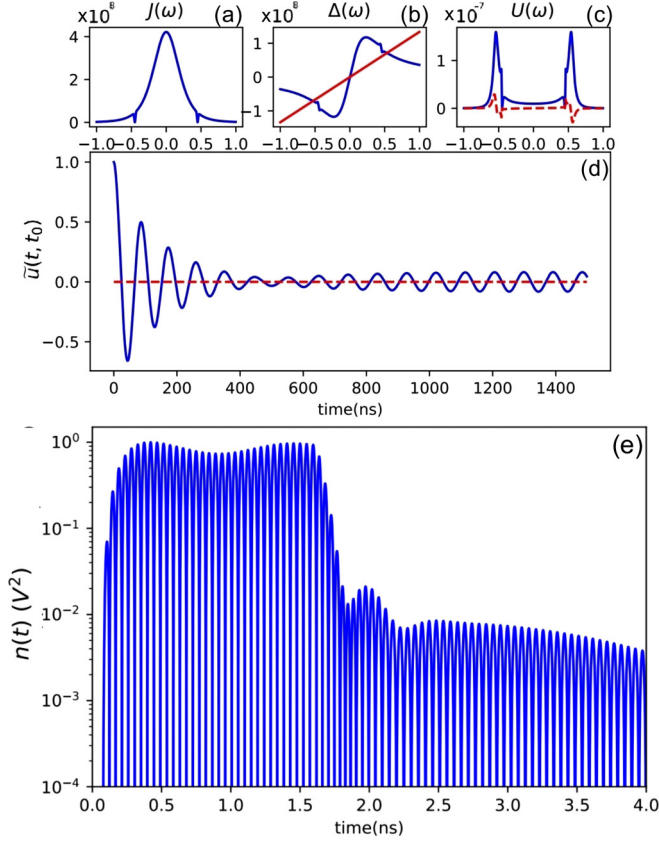


FIG. 12. (a)–(d) The same plot as Fig. 8 with a burning frequency at $\omega = \omega_s \pm (\frac{1}{2} - 0.05)\Omega_R$. (e) The corresponding cavity intensity for a sinusoidal driving field.

the spin ensemble through the spectral density $J(\omega)$. In this section, we show how the fluctuations (noises) characterize the non-Markovian memory dynamics between the cavity and the spin ensemble. To explore the memory effect, we shall study the two-time correlation functions, which measure the correlation of a past event with its future and therefore provide a physically observable definition of memory [38]. In the meantime, the two-time correlation function is now experimentally measurable in the real-time domain. In quantum optics, the familiar two-time correlation functions are the first-order and the second-order coherence functions, defined by

$$g^{(1)}(t, t + \tau) = \frac{\langle a^\dagger(t)a(t + \tau) \rangle}{\sqrt{\langle a^\dagger(t)a(t) \rangle \langle a^\dagger(t + \tau)a(t + \tau) \rangle}}, \quad (42a)$$

$$g^{(2)}(t, t + \tau) = \frac{\langle a^\dagger(t)a^\dagger(t + \tau)a(t + \tau)a(t) \rangle}{\langle a^\dagger(t)a(t) \rangle \langle a^\dagger(t + \tau)a(t + \tau) \rangle}, \quad (42b)$$

which can be calculated in terms of the functions $u(t, t_0)$, $v(\tau, t)$, and $y(t, t_0)$ in our theory. Explicitly, let $t_0 = 0$,

$$\begin{aligned} \langle a^\dagger(t)a(t + \tau) \rangle &= u^*(t)u(t + \tau)\langle a^\dagger(0)a(0) \rangle \\ &\quad + y^*(t)y(t + \tau) + v(t + \tau, t) \\ &\quad + u^*(t)y(t + \tau)\langle a^\dagger(0) \rangle \\ &\quad + u(t + \tau)y^*(t)\langle a(0) \rangle. \end{aligned} \quad (43)$$

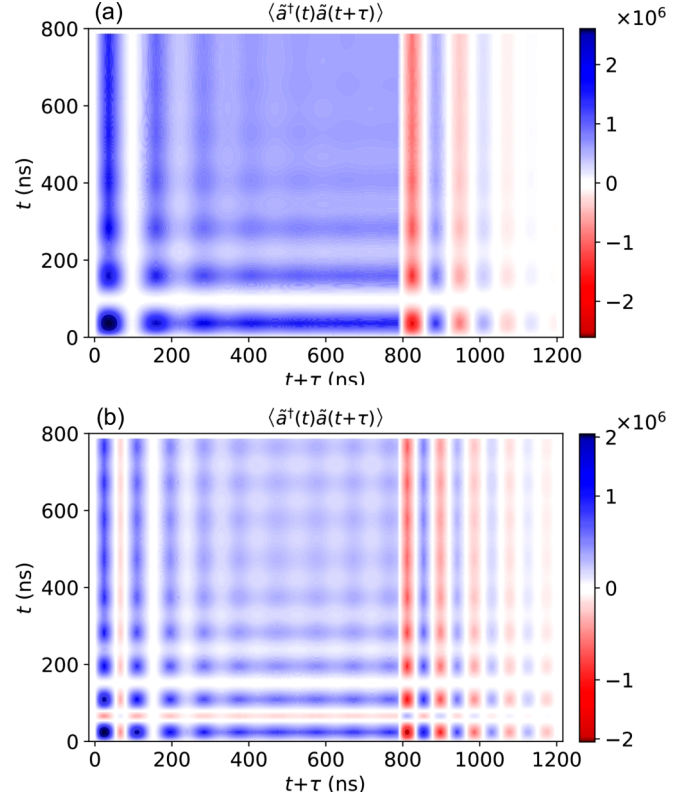


FIG. 13. The contour plot of two-time correlation function $\langle \tilde{a}^\dagger(t)\tilde{a}(t + \tau) \rangle$ under the rectangular driving field (a) in the q -Gaussian spectral density and (b) with the spectral hole burning.

The second-order correlation function is more complicated although it can still be expressed in terms of the basic Green functions $u(t)$, $v(\tau, t)$, and $y(t)$.

Here, we only present the result $\langle a^\dagger(t)a(t + \tau) \rangle$ and $g^{(1)}(t, t + \tau)$ to demonstrate the memory effect in this hybrid quantum system. Because the cavity is initially empty, the above solution is reduced to

$$\langle a^\dagger(t)a(t + \tau) \rangle = y^*(t)y(t + \tau) + v(t + \tau, t). \quad (44)$$

It shows that the coherence function is divided into two parts, the first part (the first term) is related to the coherence of the driving-field-induced cavity field at two different times, and the second term is associated with spin-ensemble-induced photon correlation. The cavity intensity studied in the previous two sections is the special case with the delay time $\tau = 0$. In Fig. 4, it shows that the driving-field-induced cavity photons dissipate into the spin ensemble in a finite timescale, then the cavity field reaches a saturation (steady state). After turning off the driving field, the remained photons in the cavity continuously dissipate into the spin ensemble, mixed with the photons retrieved back from the spin ensemble. The question to ask is how these photons coherently correlate with the photons previously injected into the cavity through the driving field.

Figure 13(a) shows the two-time correlation function $\langle a^\dagger(t)a(t + \tau) \rangle$ of the cavity field for a rectangular driving field with the same parameters used in Fig. 4. The result shows that the coherence between time t and $t + \tau$ decays

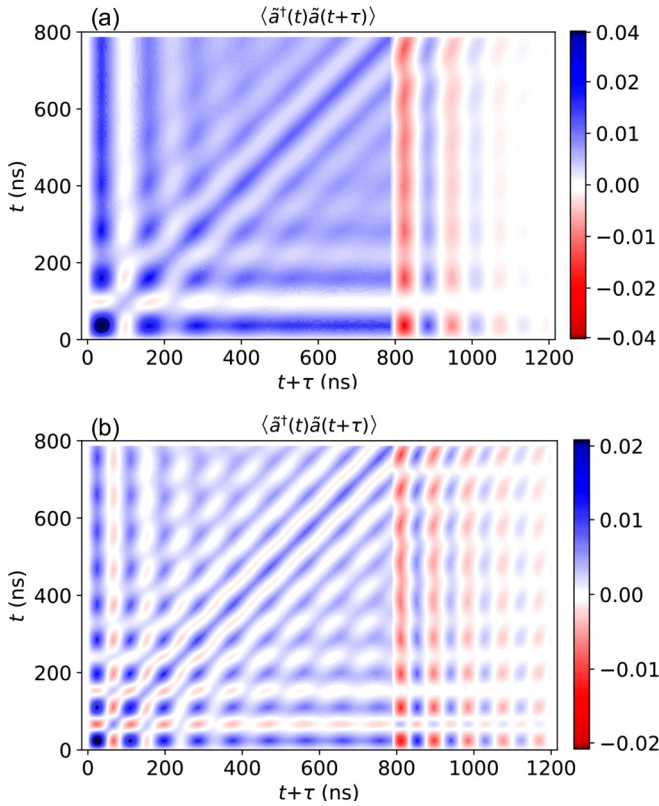


FIG. 14. The same plot as Fig. 13 with a reduced driving field amplitude by an order of 10^{-4} .

gradually before the driving field is turned off. However, once the driving field is turned off, the value of the correlation function drops to be a negative value. This negative correlation corresponds to an opposite π phase coherence between the cavity fields at time t and $t+\tau$, respectively. This is clearly shown by Eq. (34), and is manifested significantly in Fig. 13(a). Moreover, we have pointed out that this π -phase shift of the cavity field at a later time turns out a reduction of the damping oscillation period time by a half, which is also clearly seen in Fig. 13(a). On the other hand, Fig. 13(b) shows how the correlation function is changed by the spectral hole burning. The coherence behavior with the spectral hole burning obviously lasted much longer, which indicates that the spectral hole burning can effectively suppress the decoherence and maintain the cavity field coherence for a longer time.

However, the correlation functions shown in Fig. 13 are actually dominated by the classical coherences or classical correlations because the cavity field contains a large number of photons (the order of $\sim 10^6$) which is in the classical regime. To make the quantum coherence manifest, one should use a very weak driving field that maybe only contains one photon or less. The results are presented in Fig. 14. As one can see, after reducing the driving field amplitude by an order of 10^{-4} (about the single-photon regime), the two-time correlations are significantly changed. This change is mainly because the quantum noise correlation given by $v(t, t+\tau)$ becomes no longer negligible. The diagonal fringes in Fig. 14 are the manifestation of this quantum noise correlation.

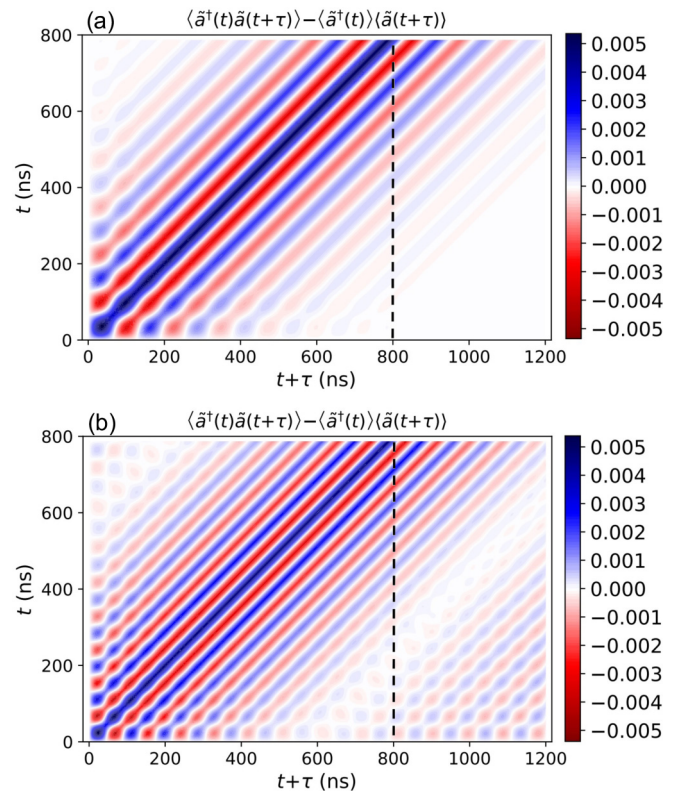


FIG. 15. The contour plot of two-time quantum correlation function (subtracting the classical part) with (a) the q -Gaussian spectrum. (b) The spectral hole burning.

To see more clearly the quantum correlations, we plot the noise correlation alone by subtracting the classical part

$$\langle a^\dagger(t)a(t+\tau) \rangle - \langle a^\dagger(t) \rangle \langle a(t+\tau) \rangle = v(t+\tau, t). \quad (45)$$

The result is presented in Fig. 15. Actually the quantum noise correlation itself is independent from the driving field, it manifests the quantum memory effect between the cavity system and the spin ensemble, and is sensitive to the spectral structure of the spin ensemble. Figures 15(a) and 15(b) show a clear difference of the quantum correlations between the q -Gaussian spectrum and the corresponding spectral hole burning. As one can see from Fig. 15(a), without spectral hole burning, there is no obvious quantum correlation for the injected cavity field with the cavity field after the driving field turned off. But, with the spectral hole burning, the spin-ensemble-induced decoherence is suppressed and quantum memory can be maintained, which is displayed by the fringes in the right-bottom corner in Fig. 15(b). It shows a long-time correlation or a long-time quantum memory effect in this hybrid quantum systems, which should be interest to measure in further experiments.

To further examine the average quantum correlations per photon and the photon-number dependence of decoherence suppression, we plot in Fig. 16 the normalized correlation function, i.e., the first-order coherence function $g^{(1)}(t, t+\tau)$ of Eq. (42a), to see the role of the quantum fluctuations and the relevant mechanism of decoherence suppression that may alter in the regimes of large and small photons. The result plotted in Fig. 16(a) corresponds to the large photon-number regime, the same case as that plotted in Fig. 13(a). By

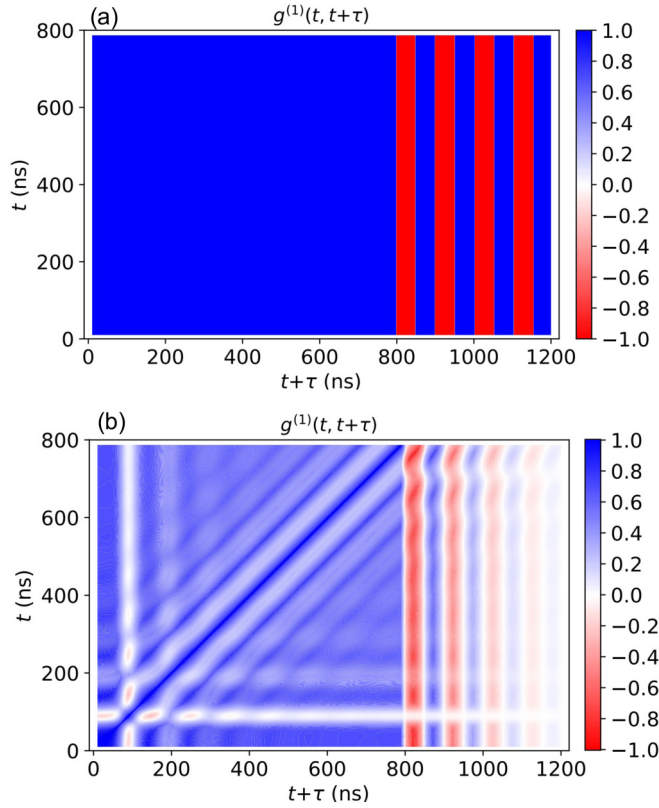


FIG. 16. The contour plot of the first-order coherence function $g^{(1)}(t, t + \tau)$ (a) with the driving field strength $\sim 10^6$ as shown in Fig. 13(a), (b) with the reduced driving field amplitude by an order of 10^{-4} , as shown in Fig. 14(a).

comparing the results of Figs. 16(a) and 13(a), one sees that the correlation patterns look quite different. However, the correlation properties in two plots are indeed similar. The result of Fig. 16(a) can be easily obtained from the fact that in the large photon-number regime (the classical field regime) where the driving field contains about 10^6 photons so that quantum fluctuations $v(t, t + \tau,)$ can be negligible [see Figs. 3(a) and 3(b)]. Thus, for the large photon-number regime, the correlation function (45) is simply reduced to

$$\langle a^\dagger(t)a(t + \tau) \rangle \simeq y^*(t)y(t + \tau). \quad (46)$$

As a result, the first-order coherent function $g^{(1)}(t, t + \tau)$ of Eq. (42a) becomes

$$g^{(1)}(t, t + \tau) \simeq \frac{y^*(t)y(t + \tau)}{|y(t)||y(t + \tau)|} \quad (47)$$

which equals to 1 before the driving field is turned off, and oscillates between ± 1 after the driving field is turned off, as shown precisely by Fig. 16(a). In other words, $g^{(1)}(t, t + \tau)$ clearly shows that in the large photon-number regime, there is no quantum correlation or, more precisely speaking, the correlation per photon is negligible between the cavity fields before and after the driving field is turned off, as has also been shown by Fig. 15(a).

On the other hand, when the driving field strength is reduced to a small photon number (quantum regime), the quantum fluctuations $v(t, t + \tau,)$ cannot be negligible so that

the simplified formula (47) is no longer valid. We plot the first-order coherence function $g^{(1)}(t, t + \tau)$ in Fig. 16(b) where the driving field is reduced by an order of 10^{-4} . By comparing the results plotted in Figs. 14(a) and 16(b), it shows that $g^{(1)}(t, t + \tau)$ and $\langle a^\dagger(t)a(t + \tau) \rangle$ provide very similar correlation properties in the small photon-number (quantum) regime, where the noise correlation or quantum memory effect is dominated. This shows how noise correlation provides indeed a quantitative description of quantum memory, as we discussed in details in Sec. IID. Through the study of two-time correlation functions, one can see the big difference of the quantum and classical correlations.

VI. DISCUSSIONS AND PERSPECTIVES

In conclusion, we provide a master equation approach to study the decoherence dynamics of the hybrid quantum systems consisting of a microwave cavity strongly coupled with an inhomogeneous broadening spin ensemble. The spin ensemble is made by negatively charged nitrogen-vacancy (NV) defects in diamond. Under the experimental condition that fewer spins ($\sim 10^6$) are excited for a large spin ($\sim 10^{12}$) ensemble, the spin ensemble can be treated by a bosonic ensemble under the Holstein-Primakoff approximation, and from which we can derive the exact master equation for the cavity system. Our exact master equation describes the transient dynamics of the cavity system under the control of the external driving field in both the classical and the quantum regimes. The study of non-Markovian decoherence dynamics of the cavity coupled strongly to the spin ensemble is reduced to solve the Green functions $u(t, t_0)$, $v(\tau, t)$ and the response function $y(t, t_0)$ with respect to the driving field, as given explicitly by Eqs. (12) and (32). These Green functions can be analytically solved. Thus, the exact master equation and the corresponding exact results depict explicitly the detailed dissipation, quantum and thermal fluctuations, quantum correlations, and quantum memory effects in a rather complete manner that other approaches cannot provide.

We apply the theory to the experiments by Putz *et al.* [29,30] and interpret the corresponding experimental observation. The experimental observations have also been described with the semiclassical mean-field approach in terms of the Volterra integral equation in [29,30]. Our results lead to a clearer and complete physical picture of the non-Markovian decoherence. In particular, we find that the suppression of the decoherence in the strong-coupling regime is due to the rapid forward and backward photon flows between the cavity and the spin ensemble arising from the symmetric spectral densities of open systems, and such phenomena are not limited to cavity systems. The rapid forward and backward photon flows, as a typical non-Markovian decoherence effect, become faster with the coupling increasing, as manifested by the rapid oscillations between huge positive and negative values for time-dependent decay coefficient $\gamma(t, t_0)$ given in the exact master equation, which also characterize the transient non-Markovian decoherence dynamics. Moreover, we find that the further suppression of decoherence through spectral hole burning [30] is due to the fact that the hole-burning spectral density generates localized bound states which is dissipationless and can significantly suppress decoherence. The

latter is indeed the general and the most efficient mechanism to suppress decoherence through long-time non-Markovian dynamics [27], and may have potential applications for the further development for quantum information technology.

We further show that the quantum memory in this hybrid quantum system can be quantified with the two-time correlation functions. From a measurement perspective, the correlation between past events and their future is a physically clear and experimentally measurable memory quantity. We study the two-time correlation function and the first-order coherence function, and show how the cavity field correlated each other before and after the driving field turned off. In particular, we show how the quantum correlation or quantum memory can be manifested in the correlation function in the quantum regime with a low driving field intensity, which can be measured in further experiments. Furthermore, based on our exact master equation, we can solve explicitly the reduced

density matrix of the cavity field in this system [see, for example, Eq. (26)], from which one can further study how the quantum states is stored in the spin ensemble and if one can retrieve them back in a later time through the experimental study with quantum state tomography [22]. Also, as an experimentally realized strong-coupling hybrid quantum system, it will be very interesting to study the strong-coupling quantum thermodynamics and its potential application for quantum heat engines with the exact master equation theory [55–57]. These will be our next research.

ACKNOWLEDGMENTS

We thank Y.-W. Huang and W.-M. Huang for helpful discussions. This work is supported by Ministry of Science and Technology of Taiwan under Contract No. MOST-108-2112-M-006-009-MY3.

-
- [1] S. Haroche and J. M. Raimond, *Exploring the Quantum: Atoms, Cavities, and Photons* (Oxford University Press, New York, 2006).
- [2] H. J. Carmichael, *An Open Systems Approach to Quantum Optics*, Lecture Notes in Physics m18 (Springer, Berlin, 1993).
- [3] H. J. Kimble and T. W. Lynn, *Cavity QED with Strong Coupling - Toward the Deterministic Control of Quantum Dynamics*, Coherence and Quantum Optics VIII, edited by Bigelow *et al.* (Kluwer Academic, New York, 2003).
- [4] Y. Kaluzny, P. Goy, M. Gross, J. M. Raimond, and S. Haroche, Observation Of Self-Induced Rabi Oscillations In Two-Level Atoms Excited Inside A Resonant Cavity: The Ringing Regime Of Superradiance, *Phys. Rev. Lett.* **51**, 1175 (1983).
- [5] M. Brune, F. Schmidt-Kaler, A. Maali, J. Dreyer, E. Hagley, J. M. Raimond, and S. Haroche, Quantum Rabi Oscillation: A Direct Test of Field Quantization In A Cavity, *Phys. Rev. Lett.* **76**, 1800 (1996).
- [6] R. J. Thompson, G. Rempe, and H. J. Kimble, Observation Of Normal-Mode Splitting For An Atom In An Optical Cavity, *Phys. Rev. Lett.* **68**, 1132 (1992).
- [7] C. J. Hood, M. S. Chapman, T. W. Lynn, and H. J. Kimble, Real-Time Cavity QED With Single Atoms, *Phys. Rev. Lett.* **80**, 4157 (1998).
- [8] J. McKeever, A. Boca, A. D. Boozer, R. Miller, J. R. Buck, A. Kuzmich, and H. J. Kimble, Deterministic generation of single photons from one atom trapped in a cavity, *Science* **303**, 1992 (2004).
- [9] A. Wallraff, D. I. Schuster, A. Blais, L. Frunzio, R.-S. Huang, J. Majer, S. Kumar, S. M. Girvin, and R. J. Schoelkopf, Strong coupling of a single photon to a superconducting qubit using circuit quantum electrodynamics, *Nature (London)* **431**, 162 (2004).
- [10] I. Chiorescu, P. Bertet, K. Semba, Y. Nakamura, C. J. P. M. Harmans, and J. E. Mooij, Coherent dynamics of a flux qubit coupled to a harmonic oscillator, *Nature (London)* **431**, 159 (2004).
- [11] Z. L. Xiang, S. Ashhab, J. Q. You, and F. Nori, Hybrid quantum circuits: superconducting circuits interacting with other quantum systems, *Rev. Mod. Phys.* **85**, 623 (2013).
- [12] R. Amsüss, Ch. Koller, T. Nöbauer, S. Putz, S. Rotter, K. Sandner, S. Schneider, M. Schramböck, G. Steinhäuser, H. Ritsch, J. Schmiedmayer, and J. Majer, Cavity QED With Magnetically Coupled Collective Spin States, *Phys. Rev. Lett.* **107**, 060502 (2011).
- [13] Y. Kubo, C. Grezes, A. Dewes, T. Umeda, J. Isoya, H. Sumiya, N. Morishita, H. Abe, S. Onoda, T. Ohshima, V. Jacques, A. Dréau, J.-F. Roch, I. Diniz, A. Auffèves, D. Vion, D. Esteve, and P. Bertet, Hybrid Quantum Circuit With A Superconducting Qubit Coupled To A Spin Ensemble, *Phys. Rev. Lett.* **107**, 220501 (2011).
- [14] S. Probst, H. Rotzinger, S. Wünsch, P. Jung, M. Jerger, M. Siegel, A. V. Ustinov, and P. A. Bushev, Anisotropic Rare-Earth Spin Ensemble Strongly Coupled To A Superconducting Resonator, *Phys. Rev. Lett.* **110**, 157001 (2013).
- [15] H. Huebl, C. W. Zollitsch, J. Lotze, F. Hocke, M. Greifenstein, A. Marx, R. Gross, and S. T. B. Goennenwein, High Cooperativity In Coupled Microwave Resonator Ferrimagnetic Insulator Hybrids, *Phys. Rev. Lett.* **111**, 127003 (2013).
- [16] Y. Tabuchi, S. Ishino, T. Ishikawa, R. Yamazaki, K. Usami, and Y. Nakamura, Hybridizing Ferromagnetic Magnons And Microwave Photons In The Quantum Limit, *Phys. Rev. Lett.* **113**, 083603 (2014).
- [17] P. L. Stanwix, L. M. Pham, J. R. Maze, D. Le Sage, T. K. Yeung, P. Cappellaro, P. R. Hemmer, A. Yacoby, M. D. Lukin, and R. L. Walsworth, Coherence of nitrogen-vacancy electronic spin ensembles in diamond, *Phys. Rev. B* **82**, 201201(R) (2010).
- [18] Z. Kurucz, J. H. Wesenberg, and K. Mølmer, Spectroscopic properties of inhomogeneously broadened spin ensembles in a cavity, *Phys. Rev. A* **83**, 053852 (2011).
- [19] I. Diniz, S. Portolan, R. Ferreira, J. M. Gérard, P. Bertet, and A. Auffèves, Strongly coupling a cavity to inhomogeneous ensembles of emitters: Potential for long-lived solid-state quantum memories, *Phys. Rev. A* **84**, 063810 (2011).
- [20] K. Sandner, H. Ritsch, R. Amsüss, Ch. Koller, T. Nöbauer, S. Putz, J. Schmiedmayer, and J. Majer, Strong magnetic coupling of an inhomogeneous nitrogen-vacancy ensemble to a cavity, *Phys. Rev. A* **85**, 053806 (2012).

- [21] M. H. Wu, C. U. Lei, W. M. Zhang, and H. N. Xiong, Non-Markovian dynamics of a microcavity coupled to a waveguide in photonic crystals, *Opt. Express* **18**, 18407 (2010).
- [22] C. U. Lei and W. M. Zhang, Decoherence suppression of open quantum systems through a strong coupling to non-Markovian reservoirs, *Phys. Rev. A* **84**, 052116 (2011).
- [23] S. B. Xue, R. B. Wu, W. M. Zhang, J. Zhang, C. W. Li, and T. J. Tarn, Decoherence suppression via non-Markovian coherent feedback control, *Phys. Rev. A* **86**, 052304 (2012).
- [24] M. W. Y. Tu and W. M. Zhang, Non-Markovian decoherence theory for a double-dot charge qubit, *Phys. Rev. B* **78**, 235311 (2008).
- [25] H. N. Xiong, W. M. Zhang, X. Wang, and M. H. Wu, Exact non-Markovian cavity dynamics strongly coupled to a reservoir, *Phys. Rev. A* **82**, 012105 (2010).
- [26] C. U. Lei and W. M. Zhang, A quantum photonic dissipative transport theory, *Ann. Phys.* **327**, 1408 (2012).
- [27] W. M. Zhang, P. Y. Lo, H. N. Xiong, M. W. Y. Tu, and F. Nori, General Non-Markovian Dynamics Of Open Quantum Systems, *Phys. Rev. Lett.* **109**, 170402 (2012).
- [28] W. M. Zhang, Exact master equation and general non-Markovian dynamics in open quantum systems, *Eur. Phys. J. Spec. Top.* **227**, 1849 (2019).
- [29] S. Putz, D. O. Krimer, R. Amsüss, A. Valookaran, T. Nöbauer, J. Schmiedmayer, S. Rotter, and J. Maje, Protecting a spin ensemble against decoherence in the strong-coupling regime of cavity QED, *Nat. Phys.* **10**, 720 (2014).
- [30] S. Putz, A. Angerer, D. O. Krimer, R. Glattauer, W. J. Munro, S. Rotter, J. Schmiedmayer, and J. Majer, Spectral hole burning and its application in microwave photonics, *Nat. Photonics* **11**, 36 (2017).
- [31] D. O. Krimer, M. Liertzer, S. Rotter, and H. E. Türeci, Route from spontaneous decay to complex multimode dynamics in cavity QED, *Phys. Rev. A* **89**, 033820 (2014).
- [32] D. O. Krimer, S. Putz, J. Majer, and S. Rotter, Non-Markovian dynamics of a single-mode cavity strongly coupled to an inhomogeneously broadened spin ensemble, *Phys. Rev. A* **90**, 043852 (2014).
- [33] D. O. Krimer, B. Hartl, and S. Rotter, Hybrid Quantum Systems With Collectively Coupled Spin States: Suppression Of Decoherence Through Spectral Hole Burning, *Phys. Rev. Lett.* **115**, 033601 (2015).
- [34] D. O. Krimer, M. Zens, S. Putz, and S. Rotter, Sustained photon pulse revivals from inhomogeneously broadened spin ensembles, *Laser Photonics Rev.* **10**, 1023 (2016).
- [35] M. Tavis and F. W. Cummings, Exact solution for an N-molecule-radiation-field Hamiltonian, *Phys. Rev.* **170**, 379 (1968).
- [36] H. Primakoff and T. Holstein, Many-body interactions in atomic and nuclear systems, *Phys. Rev.* **55**, 1218 (1939).
- [37] A. I. Lvovsky, B. C. Sanders, and W. Tittel, Optical quantum memory, *Nat. Photonics* **3**, 706 (2009).
- [38] M. M. Ali, P. Y. Lo, M. W. Y. Tu, and W. M. Zhang, Non-Markovianity measure using two-time correlation functions, *Phys. Rev. A* **92**, 062306 (2015).
- [39] M. M. Ali and W. M. Zhang, Nonequilibrium transient dynamics of photon statistics, *Phys. Rev. A* **95**, 033830 (2017).
- [40] P. Y. Yang, C. Y. Lin, and W. M. Zhang, Transient current-current correlations and noise spectra, *Phys. Rev. B* **89**, 115411 (2014).
- [41] P. Y. Lo, H. N. Xiong, and W. M. Zhang, Breakdown of Bose-Einstein distribution in photonic crystals, *Sci. Rep.* **5**, 9423 (2015).
- [42] P. Y. Yang and W. M. Zhang, Master equation approach to transient quantum transport in nanostructures, *Front. Phys.* **12**, 127204 (2017).
- [43] P. Y. Yang and W. M. Zhang, Buildup of Fano resonances in time-domain in a double quantum dot Aharonov-Bohm interferometer, *Phys. Rev. B* **97**, 054301 (2018).
- [44] H. L. Lai, Y. W. Huang, P. Y. Yang, and W. M. Zhang, Exact master equation and non-Markovian decoherence dynamics of Majorana zero modes under gate-induced charge fluctuations, *Phys. Rev. B* **97**, 054508 (2018).
- [45] W. M. Zhang, D. H. Feng, and R. Gilmore, Coherent states: Theory and some applications, *Rev. Mod. Phys.* **62**, 867 (1990).
- [46] H. T. Tan and W. M. Zhang, Non-Markovian dynamics of an open quantum system with initial system-reservoir correlations: A nanocavity coupled to a coupled-resonator optical waveguide, *Phys. Rev. A* **83**, 032102 (2011).
- [47] P. Y. Yang, C. Y. Lin, and W. M. Zhang, Master equation approach to transient quantum transport in nanostructures incorporating initial correlations, *Phys. Rev. B* **92**, 165403 (2015).
- [48] U. Weiss, *Quantum Dissipative Systems*, 3rd ed. (World Scientific, Singapore, 2008).
- [49] H. N. Xiong, P. Y. Lo, W. M. Zhang, D. H. Feng, and F. Nori, Non-Markovian complexity of quantum-to-classical transition, *Sci. Rep.* **5**, 13353 (2015).
- [50] H.-P. Breuer, E.-M. Laine, and J. Piilo, Measure For The Degree Of Non-Markovian Behavior Of Quantum Processes In Open Systems, *Phys. Rev. Lett.* **103**, 210401 (2009).
- [51] D. Chruściński and S. Maniscalco, Degree Of Non-Markovianity Of Quantum Evolution, *Phys. Rev. Lett.* **112**, 120404 (2014).
- [52] L. Viola, E. Knill, and S. Lloyd, Dynamical Decoupling Of Open Quantum Systems, *Phys. Rev. Lett.* **82**, 2417 (1999).
- [53] W. Yang, Z. Y. Wang, and R. B. Liu, Preserving qubit coherence by dynamical decoupling, *Front. Phys.* **6**, 2 (2010).
- [54] M. Fleischhauer and M. D. Lukin, Dark-State Polaritons In Electromagnetically Induced Transparency, *Phys. Rev. Lett.* **84**, 5094 (2000); Quantum memory for photons: Dark-state polaritons, *Phys. Rev. A* **65**, 022314 (2002).
- [55] F. L. Xiong and W. M. Zhang, Exact dynamics and thermalization of open quantum systems coupled to reservoirs through particle exchanges, *Phys. Rev. A* **102**, 022215 (2020).
- [56] M. Ali, W. M. Huang, and W. M. Zhang, Quantum thermodynamics of single particle systems, *Sci. Rep.* **10**, 13500 (2020).
- [57] W. M. Huang and W. M. Zhang, Strong Coupling Quantum Thermodynamics with Renormalized Hamiltonian and Temperature, [arXiv:2010.01828](https://arxiv.org/abs/2010.01828).